Stability analysis on two single-phase coupled natural circulation loops

International Journal of Heat and Mass Transfer 232 (2024) 125886

Contents lists available at ScienceDirect

International Journal of Heat and Mass Transfer

journal homepage: www.elsevier.com/locate/hmt

Stability analysis on two single-phase coupled natural circulation loops

Elia Novarese [a,1], Gabriele Benzoni [b,1], Carolina Introini [b,1], Stefano Lorenzi [b,1], Laura Savoldi [a,1], Antonio Cammi [b,*,1]

[a] MAHTEP Group, Dipartimento Energia, Politecnico di Torino, 10124, Torino, Italy
[b] Department of Energy, Politecnico di Milano, via la Masa 34, 20156, Milano, Italy

ARTICLE INFO

Keywords:
Coupled natural circulation loops
DYNASTY-eDYNASTY
1D modelling
Steady-state analysis
Stability maps

ABSTRACT

In designing Molten Salt Reactors, implementing passive safety systems that rely on natural circulation phenomena can be an attractive proposal to remove decay heat from the core. In this type of reactor, when the active cooling system fails, the fuel-coolant salt flows by natural circulation in the presence of Internal Heat Generation due to the fuel dissolved and mixed within the coolant salt. Adopting a Natural Circulation Loop for the dissipation of the heat generated can be an attractive safety system, but it is affected by some undesired phenomena regarding flow mass rate oscillation, which influences the heat transfer efficiency and local temperature. In particular, it is necessary to understand the influence of the Natural Circulation loop on the internal stability of the reactor. The purpose of the DYNASTY-eDYNASTY facility (DYnamics of NAtural circulation for molten SalT internallY heated), built at Politecnico di Milano, is to investigate the dynamical effects manifesting in a Coupled Natural Circulation Loops and to get insights about the phenomenology which can result relevant for the study of accidental scenarios in Molten Salt Reactors, simulating the natural circulation in the reactor and the Natural Circulation Loop of the passive safety system. This paper, starting from the one-dimensional model of the DYNASTY-eDYNASTY facility, develops a in-house code for the computation of the steady states and a Stability Map for the stability analysis of the Coupled Natural Circulation Loops. Verification of the results has been carried out by comparing the outcomes derived from the MODELICA model of the DYNASTY-eDYNASTY facility adopting the DYMOLA® environment. The steady-state model can predict the results of the DYMOLA® simulations with acceptable accordance, and the verification of the Stability Map with DYMOLA® simulations highlighted a good prediction of the model developed for the stability analysis.

1. Introduction

In the last decade, a renewed interest in the nuclear energy sector has made it possible to focus part of the research on the safety of the Nuclear Power Plant. Recently, new reactor designs include passive safety features for various purposes, such as core cooling during transients, design basis accidents or severe accidents or containment cooling [1]. Passive safety systems that exploit the natural circulation of the coolant fluid to transfer heat from a hot source to a cold sink are more attractive than those which adopt forced convection [2] as they rely on general physical laws. In the presence of density gradients induced by temperature differences, convective motion can be self-sustained [2,3], avoiding adopting active components [4]. Natural Circulation Loops (NCLs) are systems employed to investigate the phenomenon of natural circulation or as passive safety systems for heat removal. These systems can be subjected to instabilities and dynamic oscillations [2,4–6] which can compromise heat removal efficiency and the fluid could reach a local temperature which could not be compatible with the materials used. These instabilities rise from the competition between the buoyancy forces driving the fluid and the friction forces, which hinder the fluid motion [7,8]. Moreover, NCLs are also affected by the pipe-wall material: Cammi et al. [2] have highlighted how its thermal capacity and conductivity tend to stabilize the dynamics of the system. In this context, having reliable models that can predict the behaviour of this phenomenon is of particular interest in the design of safety systems based on natural circulation. One task of the Generation IV Molten Salt Fast Reactors is to ensure a high level of safety also during the occurrence of an accident [9]: the reactor is designed to allow the natural circulation of the coolant when the power supply of

* Corresponding author.
E-mail addresses: elia.novarese@polito.it (E. Novarese), gabriele.benzoni@polimi.it (G. Benzoni), carolina.introini@polimi.it (C. Introini), stefano.lorenzi@polimi.it (S. Lorenzi), laura.savoldi@polito.it (L. Savoldi), antonio.cammi@polimi.it (A. Cammi).
[1] The authors contributed equally to this work.

https://doi.org/10.1016/j.ijheatmasstransfer.2024.125886
Received 14 February 2024; Received in revised form 20 June 2024; Accepted 21 June 2024
Available online 10 July 2024

Nomenclature

Latin symbols

$\hat{\mathbf{e}}_s$	Unit vector following the fluid flow (dimensionless)
$\hat{\mathbf{e}}_z$	Unit vector pointing towards the positive vertical direction (dimensionless)
$\mathcal{L}_{eq}$	Thermal barycentre distance (m)
$\tilde{R}$	Thermal resistance (m K W^{-1})
$\tilde{S}$	Lateral surface of an infinitesimal shell of the pipe (m^2)
$\tilde{s}$	Length of an infinitesimal shell of the pipe (m)
$\tilde{V}$	Volume of a infinitesimal shell pipe (m^3)
a	Auxiliary constant for temperature profile at heat exchanger (dimensionless)
B	Parameter describing the effect of the heat exchange (dimensionless)
b	Auxiliary constant for temperature profile at cooler (dimensionless)
c	Specific heat (J kg^{-1} K^{-1})
D	Diameter (m)
g	Gravitational acceleration (m s^{-1})
h	Heat transfer coefficient (W m^{-2} K^{-1})
k	Thermal conductivity (W m^{-1} K^{-1})
L	DYNASTY length (m)
l	eDYNASTY length (m)
L_{tot}	Loop total length (m)
Nu	Nusselt number (dimensionless)
p	Pressure (Pa)
Pr	Prandtl number (dimensionless)
q''	Heat flux (W m^{-2})
Q	Heat power (W)
Re	Reynolds number (dimensionless)
s	Curvilinear coordinate (m)
St_m	Modified Stanton number (dimensionless)
T	Temperature (K)
t	Time (s)
u	Fluid velocity (m s^{-1})

Greek symbols

α	Auxiliary exponent in heat exchanger temperature field (m^{-1})
β	Auxiliary exponent in cooler temperature field (m^{-1})
β_f	Fluid thermal expansion coefficient (K^{-1})
Δ	Finite variation of a parameter (dimensionless)
δ	Infinitesimal variation of a parameter (dimensionless)
δ_{HE}	Auxiliary parameter for the heat exchanger (dimensionless)
ϵ	Inverse of the annular hydraulic diameter (m^{-1})
Γ	Mass rate (kg s^{-1})
γ	Relative mass rate error (%)
λ	Darcy friction factor (dimensionless)
μ	Dynamic viscosity (Pa s)
ω	Complex frequency of the Laplace transform (s^{-1})
Ψ	Fermi–Dirac interpolation function (dimensionless)
ρ	Mass density (kg m^{-1})
τ_w	Wall thickness (m)

Subscripts–superscripts

*	Reference value
$_0$	Steady-state
$^-$	Dimensionless variable
$_{DYM}$	DYMOLA
$_{Py}$	Python
$_1$	DYNASTY loop
$_2$	eDYNASTY loop
$_f$	Fluid
$_w$	Wall
$_{conc}$	Concentrated
$_{COOL}$	Cooler
$_{distrib}$	Distributed
$_{fric}$	Frictional
$_{HE}$	Heat Exchanger
$_H$	Heater
$_j$	jth loop ($j = 1, 2$)
$_P$	Adiabatic pipe
$_{w_i}$	Inner wall shell
$_{w_o}$	Outer wall shell

Acronyms

CNCLs	Coupled Natural Circulation Loops
DH	Distributed Heating
DYNASTY	DYnamics of NAtural circulation for molten SalT internallY heated
EHS	External Heat Source
HE	Heat Exchanger
IDE	Integrated Development Environment
IHG	Internal Heat Generation
MSR	Molten Salt Reactor
NCL	Natural Circulation Loop
ODE	Ordinary Differential Equation
PRHR	Passive Residual Heat Removal Systems
SCNL	Single Natural Circulation Loop

the pumps is lost, and a safety system based on NCL must work properly and efficiently to dissipate the heat generated in the core. Moreover, this particular type of reactor introduces the concept of the Internal Heat Generation (IHG) for the coolant: the fluid which flows in the core reactor is a homogeneous mixture of molten salt and fissile material and acts both as coolant and fuel [10]. In the case of shutdown of the reactor, the fission products dissolved in the salt act as a density source of heat due to their radioactive decay, which must be dissipated to maintain the integrity of the reactor. Considering these characteristics of the MSFR in an accident scenario, Natural Circulation established in the reactor by IHG, the problem of instabilities that can occur within it is of particular interest and needs to be studied for future development in this field.

The DYNASTY-eDYNASTY facility (DYnamics of NAtural circulation for molten SalT internallY heated) was designed and built at Politecnico di Milano [8,11,12] for simulating the behaviour of Natural Circulation in a coupled system with a distributed heat source. The facility is

Table 1
Length dimensions for the DYNASTY-eDYNASTY model adopted in this paper.

	Subscript (j)								Total length
	1	2	3	4	5	6	C	HE	
DYNASTY loop L_j (m)	0	3.1	3.09	0.5	0.5	0.45	2.1	2.64	12.38
eDYNASTY loop l_j (m)	0.59	0.5	0.5	3.23	3.1	0	2.1	2.64	12.66

realized by two NCLs, named DYNASTY and eDYNASTY loop. DYNASTY represents the primary NCL, whose heating system is designed to simulate a loop under Internal Heat Generation conditions; this loop is coupled with eDYNASTY, which represents the secondary NCL, through a double-pipe heat exchanger. Due to the high ratio of axial length to radius of the pipes, the External Heat Source (EHS) is a good first approximation to the IHG. This avoids the difficult problems of adopting a heating system based on an IHG in favour of a distributed EHS, which is easier to manage and control during experiments.

The DYNASTY-eDYNASTY facility is unique among NCLs as it is the only one capable of investigating the coupling between two interconnected NCLs. As such, it allows the dynamics of the Natural Circulation Loop to be studied, and in particular its stability, both under heating conditions approximating IHG and in the presence of a secondary coupled loop driven by NC. This configuration is of particular interest for the MSFR reactor, as it represent the operating condition of the passive Decay Heat Removal System. Due to this uniqueness and to the peculiarity of its working conditions, the DYNASTY-eDYNASTY facility has to be studied and characterized first and foremost using well-proven methods to ensure a coherent and reliable analysis. In particular, this work adopts the well-known one-dimensional analysis and Perturbation Theory to retrieve the Stability Map characterizing the system, a necessary requirement to perform more detailed analyses and to set-up experimental campaign. On the basis of the Stability Map of the DYNASTY-eDYNASTY facility, it is possible to clear up some of the doubts that arise when two Natural Circulation Loops are coupled together. In the event of an accidental scenario occurring in the primary loop that causes instabilities to increase in its dynamics, it is important to understand whether the presence of the coupled secondary loop is able to stabilize the system. On the other hand, it is crucial to study whether the occurrence of a transient in the secondary loop can have an influence on the primary loop, affecting its stability and causing the system to become unstable.

The purpose of this paper is to extend the analytical mono-dimensional studies conducted by [2,12] for the Single Natural Circulation Loops (SCNLs), including the effect of the additional thermal inertia provided by the coupling of a secondary loop, expanding the analysis to Coupled Natural Circulation Loops (CNCLs). The particular case of the DYNASTY-eDYNASTY configuration for CNCLs is studied, obtaining its Stability Map from well-proven techniques in order to answer to the main doubts mentioned.

The paper is organized as follows. In Section 2, a brief introduction of the DYNASTY-eDYNASTY facility and the relevant dimensions adopted to conduct the analysis are presented. Section 3 introduces the dynamical mono-dimensional equations based on conservation laws to model the DYNASTY-eDYNASTY facility. In Sections 4 and 5, the models to perform steady-state and stability analysis of the CNCLs are derived. Section 6 is dedicated to presenting the simplified model of the DYNASTY-eDYNASTY facility, developed in the MODELICA language and used to perform verification of the models developed in Sections 4 and 5. In Section 7, the results obtained from the developed analytical models are verified by comparing with those obtained through the MODELICA model simulations, and in Section 8, the conclusions and possible future case studies are discussed.

2. DYNASTY-eDYNASTY facility

A complete description of the design of the DYNASTY-eDYNASTY facility has been given in [6]. Therefore, in this section, only a summary is provided.

Table 2
Pipe dimensions for the DYNASTY-eDYNASTY model adopted in this paper. The subscript 1 is for the DYNASTY loop, while subscript 2 refers to the eDYNASTY loop. For the external pipe of the heat exchanger (Fig. 2), the subscript is HE.

	Subscript (j)		
	1	2	HE
Inner diameter D_{f_j} (mm)	38.2	38.2	56
Thickness τ_{w_j} (mm)	2	2	2

The facility, built at the Energy lab of Politecnico di Milano, is composed of two rectangular Natural Circulation loops realized in stainless steel named DYNASTY loop, made of AISI 316L, and eDYNASTY loop, made of AISI 304, which are coupled through a double pipe heat exchanger. The facility can operate as an SCNL with the stand-alone DYNASTY loop, bypassing the heat exchanger through a vertical pipe, or as CNCLs with both loops. The heating system is placed in the DYNASTY loop and consists of tape of electrical resistances that envelope the horizontal bottom leg and the two vertical legs, which can be heated independently. The Distributed Heating (DH) configuration is achieved by switching on all electrical resistances and would simulate the case when the fluid is heated by Internal Heat Generation (IHG). Thanks to the high axial length-to-radius ratio of the pipe, the IHG condition can be replaced with an External Heating Source (EHS) [2], experimentally simulated with the electrical resistances enveloped to the pipes of the DYNASTY loop. The cooling system consists of two finned pipes placed in the horizontal top leg of both loops in cross-flow with a fan.

Fig. 1 shows the DYNASTY and eDYNASTY loop configured as CNCLs, where the heating system is highlighted in red, the coolers are light blue and the heat exchanger is green, and the terminology adopted for the lengths, distinguishing with the capital letter L those of the DYNASTY loop and lowercase letter l those of the eDYNASTY loop, while in Table 1 the principal length dimensions are reported. In the DYNASTY loop (Fig. 1(a)), the pump's leg is only opened when using forced circulation, closing the leg below where the mass-flow meter (Endress-Hauser® Promass F80 DN25 Coriolis, [13]) is placed. The heat exchanger is characterized by an annular cross-section, called in this paper secondary side, which is in communication with the eDYNASTY loop, and an internal pipe that is part of the DYNASTY loop, called the primary side. Fig. 2 shows the cross-section of the heat exchanger and some nomenclature adopted, while Table 2 reports the principal pipe dimensions for both loops.

3. Mathematical model

3.1. Main hypothesis

In this section, the governing equations for a generic NCL are presented. In the case of CNCLs, the same hypothesis assumed in [2] have been adopted and extended for the eDYNASTY loop. Specifically, for the working fluids:

- The flow is considered incompressible and one-dimensional along the axial direction of the pipes for both loops.
- The Boussinesq approximation is used.
- The flow regime (laminar, laminar-turbulent transition, or fully turbulent) does not change within the DYNASTY loop.

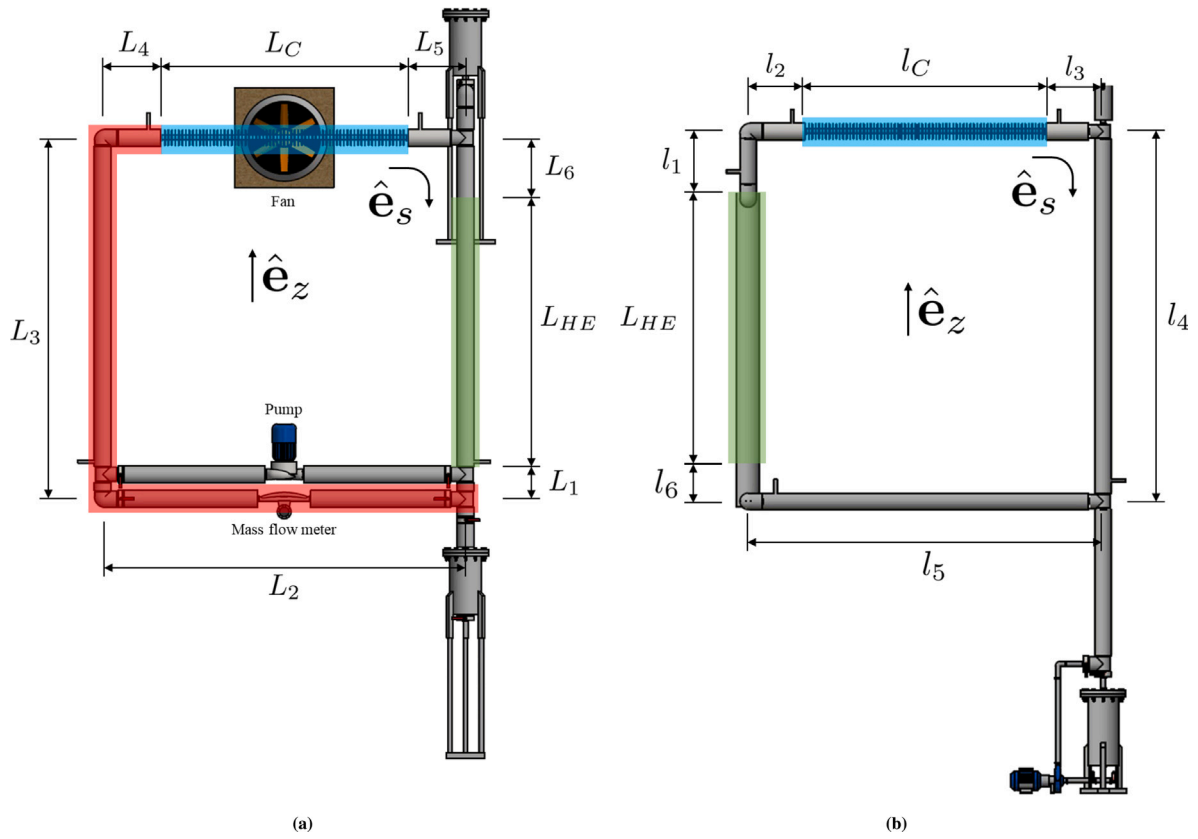

Fig. 1. (a) DYNASTY loop and (b) eDYNASTY loop with the main length nomenclature adopted and the dimensions reported in Table 1. The heater zone is highlighted in red, the coolers are in blue and the heat exchanger is in green. (For interpretation of the references to colour in this figure legend, the reader is referred to the web version of this article.)
Source: Adapted from [6].

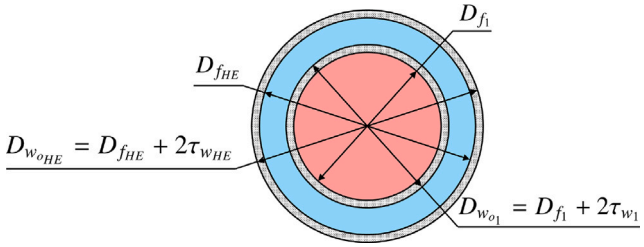

Fig. 2. Section of the heat exchanger with nomenclature. The primary side, corresponding to the cross-section of the green pipe in Fig. 1(a), is highlighted in red, whereas the secondary side, corresponding to the cross-section of the green pipe in Fig. 1(b), is shown in light blue. (For interpretation of the references to colour in this figure legend, the reader is referred to the web version of this article.)

- Conversely, eDYNASTY will see two different flow regimes, one in the annular section of the heat exchanger and another one in the rest of the loop, due to the different hydraulic diameters of the two sections.
- Dissipative and diffusion terms in the energy balance are neglected.

Regarding the solid regions characterized by the pipe walls, they have been discretized along the radial coordinate into two coaxial shells (namely, the inner and the outer wall), adopting a lumped parameter approach [2], as Fig. 3 shows.

The same hypothesis assumed by [2] for the pipe walls have been adopted:

- The wall thickness (τ_w) and the diameter ($D_{w_o} = D_f + 2\tau_w$) of the pipes are constant.
- A thermal capacitance (c_w) is assigned to each shell.
- A conductive thermal resistance ($\tilde{R}_w$) is placed between the two shells.
- The thermo-physical properties are assumed constant.
- The axial conduction and the thermal dissipations are neglected.

Regarding the thermo-physical properties of the walls, the same parameters adopted by [2] for the stainless-steel AISI 316L were used for both loops: $\rho_w = 8238\ \mathrm{kg/m^3}$ (density), $c_w = 468\ \mathrm{J/(kg\,K)}$ (specific heat), $k_w = 13.4\ \mathrm{W/(m\,K)}$ (thermal conductivity). The heater zone is modelled as a uniform heat flux source q'', while the coolers are modelled by assuming an imposed temperature T_c to the external surfaces of the walls. Regarding the cooler of the DYNASTY loop, it can also be treated as an adiabatic pipe when heat exchange in that zone is not considered. Moreover, models for the heat transfer coefficients and friction factor, based on the definition of dimensionless Nusselt, Reynolds and Prandtl numbers, have been implemented to complete the set of equations.

3.2. General equations

The governing equations are the same adopted in [2] based on the conservation laws expressed in one spatial dimension. A point along both the DYNASTY and eDYNASTY loops is identified by the curvilinear coordinate s_j, where j is the subscript equal to 1 or 2 referring to DYNASTY or eDYNASTY loops respectively, with the assumption of clockwise flow directions (Fig. 1). Two arbitrary starting points were chosen ($s_{1,2} = 0$): the entrance of the heat exchanger for the DYNASTY loop and the exit of the heat exchanger for the eDYNASTY loop (which

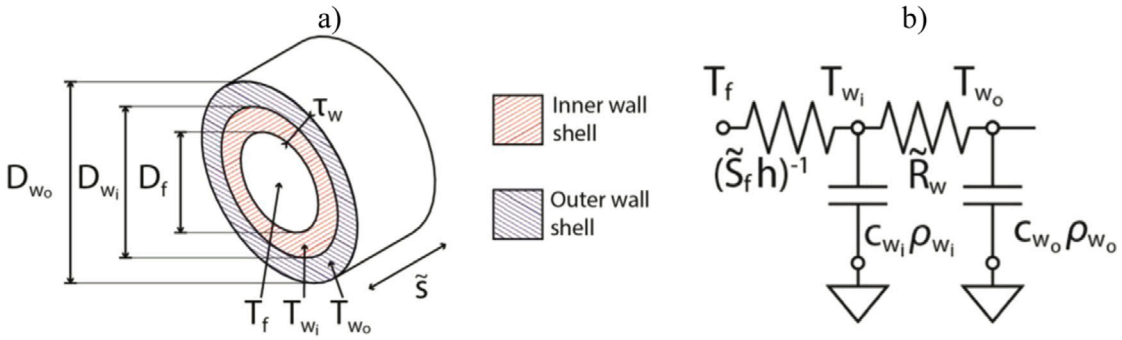

Fig. 3. (a) Discretization of the pipe wall and (b) the equivalent t scheme for thermal capacitances and resistances [2].

correspond to the top part of the heat exchanger in Fig. 1). With the hypothesis introduced in Section 3.1, Eq. (1) express the conservation laws for the fluid flows for both DYNASTY and eDYNASTY loop, except for the heat exchanger zone.[2]

$$\frac{\partial G_j}{\partial s_j} = 0 \quad \text{with} \quad G_j = \rho^*_{f_j} u_j \tag{1a}$$

$$\frac{\partial G_j}{\partial t} + \frac{\partial}{\partial s_j}\frac{G_j^2}{\rho^*_{f_j}} = -\frac{\partial p_j}{\partial s_j} - \frac{1}{2}\lambda_j \frac{G_j^2}{\rho^*_{f_j}}\frac{1}{D_{f_j}} - \rho_{f_j} g \hat{\mathbf{e}}_z \cdot \hat{\mathbf{e}}_s \tag{1b}$$

$$\rho^*_{f_j} c_{f_j} \frac{\partial T_{f_j}}{\partial t} + G_j c_{f_j} \frac{\partial T_{f_j}}{\partial s_j} = -h_{j_m}(T_{f_j} - T_{w_{i_j}})\frac{\tilde{S}_{f_j}}{\tilde{V}_{f_j}} \tag{1c}$$

The influence of the pipe walls was taken into consideration by the heat conduction Eq. (2) for the two discretized wall shells.

$$\rho_{w_j} c_{w_j} \frac{\partial T_{w_{i_j}}}{\partial t} = h_{j_m}(T_{f_j} - T_{w_{i_j}})\frac{\tilde{S}_{f_j}}{\tilde{V}_{w_{i_j}}} - \frac{T_{w_{i_j}} - T_{w_{o_j}}}{\tilde{V}_{w_{i_j}}\tilde{R}_{w_j}} \tag{2a}$$

$$\begin{cases} T_{w_{o_j}} = T_c & \text{cooler} \\ \rho_{w_j} c_{w_j}\frac{\partial T_{w_{o_j}}}{\partial t} = \frac{T_{w_{i_j}} - T_{w_{o_j}}}{\tilde{V}_{w_{o_j}}\tilde{R}_{w_j}} + \frac{\tilde{S}_{w_{o_j}}}{\tilde{V}_{w_{o_j}}} q'' & \text{heater} \\ \rho_{w_j} c_{w_j}\frac{\partial T_{w_{o_j}}}{\partial t} = \frac{T_{w_{i_j}} - T_{w_{o_j}}}{\tilde{V}_{w_{o_j}}\tilde{R}_{w_j}} & \text{otherwise} \end{cases} \tag{2b}$$

where:

$$\begin{aligned} \tilde{V}_{f_j} &= \pi\left(\frac{D_{f_j}}{2}\right)^2 \tilde{s} & \tilde{S}_{f_j} &= \pi D_{f_j}\tilde{s} \\ \tilde{V}_{w_{i_j}} &= \pi\left[\left(\frac{D_{w_{i_j}}}{2}\right)^2 - \left(\frac{D_{f_j}}{2}\right)^2\right] & \tilde{S}_{w_{i_j}} &= \pi D_{w_{i_j}}\tilde{s} \\ \tilde{V}_{w_{o_j}} &= \pi\left[\left(\frac{D_{w_{o_j}}}{2}\right)^2 - \left(\frac{D_{w_{i_j}}}{2}\right)^2\right] & \tilde{S}_{w_{o_j}} &= \pi D_{w_{o_j}}\tilde{s} \end{aligned} \tag{3}$$

Eqs. (1a) to (1c) are the mass, momentum and energy balance respectively. The infinitesimal volumes and surfaces are reported in Eq. (3). With reference to Eqs. (1) and (2), G is the mass flux, u is the velocity magnitude, ρ is the density, λ is the Darcy friction factor, p is the pressure, T is the temperature, c is the specific heat and h is the heat transfer coefficient. $\tilde{V}$ and $\tilde{S}$ stands for volume and lateral surface of an element of infinitesimal length $\tilde{s}$. The superscript * specifies the reference thermo-physical quantities for the fluid region taken at the origin of each curvilinear coordinate ($s_j = 0$) for each loop for the specific fluid (ρ^*_f is the fluid reference density, while ρ_f is the fluid density along the loop). The subscripts f and w stand for fluid and wall, respectively. In particular, w_i refers to the inner wall shell, while w_o to the outer one. g denotes gravitational acceleration, $\hat{\mathbf{e}}_z$ the z direction unit vector, and $\hat{\mathbf{e}}_s$ the flow direction unit vector. The subscript m in the heat transfer coefficient refers to the different zones of the cooler ($m = COOL$), heater ($m = H$), and adiabatic pipe ($m = P$), where the coefficients are computed with different correlations, resumed in Section 3.4. The thermal resistance $\tilde{R}_{w_j}$ is computed with equation Eq. (4):

$$\tilde{R}_{w_j} = \frac{1}{2\pi k_{w_j}\tilde{s}} log\left(\frac{D_{w_{o_j}}}{D_{f_j}}\right) \tag{4}$$

where k_{w_j} is the thermal conductivity of the wall of the jth loop.

3.3. Equations of heat exchanger

The equations for the primary side of the heat exchanger are identical to Eqs. (1) and Eq. (2a) with $j_m = 1_{HE}$, where the subscript HE refers to the heat exchanger zone. Concerning the outer wall shell equation for the primary side, the heat transferred to the secondary fluid must be included. Naming the heat transfer coefficient h_{HE}, the equation for the heat conduction of the outer wall shell of the DYNASTY loop in the heat exchanger can be expressed as Eq. (5):

$$\rho_{w_1} c_{w_1}\frac{\partial T_{w_{o_1}}}{\partial t} = \frac{T_{w_{i_1}} - T_{w_{o_1}}}{\tilde{V}_{w_{o_1}}\tilde{R}_{w_1}} + h_{HE}(T_{f_2} - T_{w_{o_1}})\frac{\tilde{S}_{w_{o_1}}}{\tilde{V}_{w_{o_1}}} \tag{5}$$

Regarding the annular cross-section, thus the secondary side of the heat exchanger, all the variables are marked with the subscript HE. The mass balance equation does not change:

$$\frac{\partial G_{HE}}{\partial s_2} = 0 \quad \text{with} \quad G_{HE} = \rho^*_{f_2} u_{HE} \tag{6}$$

The momentum equation must take into account the hydraulic diameter of the annular cross-section in the friction term, as expressed in Eq. (7):

$$\begin{aligned} \frac{\partial G_{HE}}{\partial t} + \frac{\partial}{\partial s_2}\frac{G_{HE}^2}{\rho^*_{f_2}} &= -\frac{\partial p_2}{\partial s_2} - \frac{1}{2}\lambda_{HE}\frac{G_{HE}^2}{\rho^*_{f_2}}\epsilon - \rho_{f_2} g \hat{\mathbf{e}}_z \cdot \hat{\mathbf{e}}_s \\ \text{with} \quad \epsilon &= \frac{1}{D_{f_{HE}} - (D_{f_1} + 2\tau_{w_1})} \end{aligned} \tag{7}$$

where ϵ is the inverse of the hydraulic diameter of the annulus.

Regarding the energy equation for the secondary fluid which flows through the annulus, two heat transfer coefficients h are assigned to it: one related to the heat transfer with the outer wall shell of the primary circuit (h_{HE}) and one related to the heat transfer with the external wall shell of the heat exchanger ($h_{2_{HE}}$). Thus, the energy balance can be written as Eq. (8):

$$\begin{aligned} \rho^*_{f_2} c_{f_2}\frac{\partial T_{f_2}}{\partial t} + G_{HE} c_{f_2}\frac{\partial T_{f_2}}{\partial s_2} = &- h_{HE}(T_{f_2} - T_{w_{o_1}})\frac{\tilde{S}_{w_{o_1}}}{\tilde{V}_{f_{HE}}} \\ &- h_{2_{HE}}(T_{f_2} - T_{w_{i_2}})\frac{\tilde{S}_{f_{HE}}}{\tilde{V}_{f_{HE}}} \end{aligned} \tag{8}$$

[2] As the cross-section was assumed uniform, it can be neglected in the mass conservation Eq. (1a).

where:

$$\tilde{V}_{f_{HE}} = \pi\left[\left(\frac{D_{f_{HE}}}{2}\right)^2 - \left(\frac{D_{w_{o_1}}}{2}\right)^2\right] \quad \tilde{S}_{f_{HE}} = \pi D_{f_{HE}}\tilde{s} \tag{9}$$

The inner shell of the external wall of the heat exchanger can be modelled with Eq. (10):

$$\rho_{w_2} c_{w_2} \frac{\partial T_{w_{i_2}}}{\partial t} = h_{2_{HE}}(T_{f_2} - T_{w_{i_2}})\frac{\tilde{S}_{f_{HE}}}{\tilde{V}_{w_{i_{HE}}}} - \frac{T_{w_{i_2}} - T_{w_{o_2}}}{\tilde{V}_{w_{i_{HE}}}\tilde{R}_{w_{HE}}} \tag{10}$$

The outer shell of the external wall of the heat exchanger can be modelled with Eq. (11) where heat exchange is not considered between the outer wall and the external environment.

$$\rho_{w_2} c_{w_2} \frac{\partial T_{w_{o_2}}}{\partial t} = \frac{T_{w_{i_2}} - T_{w_{o_2}}}{\tilde{V}_{w_{o_{HE}}}\tilde{R}_{w_{HE}}} \tag{11}$$

The mass fluxes of the eDYNASTY loop are linked thanks to the conservation of mass at the entrance and exit of the heat exchanger:

$$G_2\tilde{V}_{f_2} = G_{HE}\tilde{V}_{f_{HE}} \tag{12}$$

In this way the mass rates are conserved at the interfaces.

3.4. Coefficients models

The models for the Darcy friction factor and heat transfer coefficients, found in literature, are based on models defined starting from the Nusselt, Reynolds and Prandtl dimensionless numbers, defined as:

$$h = \frac{Nu \cdot k_f}{D_h} \quad Re = \frac{G \cdot D_h}{\mu_f} \quad Pr = \frac{c_f \cdot \mu_f}{k_f} \tag{13}$$

The Darcy friction factor correlation is assumed:

$$\lambda = \left(\frac{64}{Re}\right)^{\Psi_\lambda}\left(\frac{0.316}{Re^{0.25}}\right)^{1-\Psi_\lambda} \tag{14}$$

where

$$\Psi_\lambda = \left(1 + e^{\frac{Re-2530}{120}}\right)^{-1}$$

is the "Fermi–Dirac" function centred at $Re = 2530$, which is the value chosen for the transition from laminar to turbulent flow [5]. The "Fermi–Dirac" function interpolates the Darcy friction factors for the laminar and turbulent regime, allowing to adopt a unique, continuous and derivable correlation of the friction factor (Eq. (14)) for the entire Reynolds range, particularly suitable for the numerical calculation of natural circulation problems which cover a wide range of regimes. For the Nusselt number, the model adopted is the same one proposed by [4]:

$$Nu = \left[Nu_H^{\Psi_{Nu_1}}\left(Nu_S^{\Psi_{Nu_3}} Nu_G^{1-\Psi_{Nu_3}}\right)^{1-\Psi_{Nu_1}}\right]^{\Psi_{Nu_2}} \cdot \left(Nu_S^{\Psi_{Nu_3}} Nu_{DB}^{1-\Psi_{Nu_3}}\right)^{1-\Psi_{Nu_2}} \tag{15}$$

where Ψ_{Nu_1}, Ψ_{Nu_2} and Ψ_{Nu_3} are the "Fermi–Dirac" functions adopted for interpolating the correlations used for the Nusselt number in the Reynolds and Prandtl range, defined as reported in Eq. (16).

$$\Psi_{Nu_1} = \left(1 + e^{\frac{Re-2530}{20}}\right)^{-1} \tag{16a}$$

$$\Psi_{Nu_2} = \left(1 + e^{\frac{Re-10^5}{20}}\right)^{-1} \tag{16b}$$

$$\Psi_{Nu_3} = \left(1 + e^{\frac{Pr-0.6}{10^{-5}}}\right)^{-1} \tag{16c}$$

$Nu_H, Nu_S, Nu_G, Nu_{DB}$ are respectively the Hausen, Skupinski, Gnielinski and Dittus–Boelter correlations for the Nusselt number [14], summarized in Table 3. The Hausen correlation is suitable for the cooler zone [14] for the laminar regime and imposed temperature at the wall of the pipe. Regarding the heater zone, where uniform heat flux is imposed and not the temperature, the Hausen correlation is replaced with the analytical solution $Nu = \frac{48}{11}$ [14], reported in Table 3.

4. Steady-state analysis

Starting from the set of dynamic Eqs. (1) and (2) for the DYNASTY and eDYNASTY loop, and Eqs. (5) to (8), (10) and (11) for the heat exchanger, the steady state was obtained neglecting the partial time derivative. In this way, a set of Ordinary Differential Equations (ODEs) was obtained for each pipe that composes the CNCLs. The temperature field solution was first obtained in Section 4.1, and then the momentum equations were integrated along each loop to obtain a global balance of the forces that act on the fluid and allow natural circulation (Section 4.2). All the quantities obtained from solving the steady-state equation are indicated with a superscript 0.

4.1. Temperature fields

The fluid temperature profile of each NCL can be derived by solving Eqs. (1c), (2), (5), (8), (10) and (11) expressed in steady-state form. Thanks to the ODEs obtained, it is possible to obtain the temperature along the coolers, heater and each adiabatic pipe. To make equations more compact and readable, the following quantities were defined:

$$\Delta T^0 = \frac{Q}{\Gamma_1 c_{f_1}} \quad Q = q''\frac{\tilde{S}_{w_{o_1}}}{\tilde{s}}L_H \quad \Gamma_j = G_j\frac{\tilde{V}_{f_j}}{\tilde{s}} \tag{17}$$

where ΔT^0 is the primary fluid temperature difference between the outlet and the inlet of the heater, Q is the total power delivered by the heater, L_H is the heater length and Γ_j is the mass rate of each loop. In this way, the analytical temperature fields for the regions of the cooler, the adiabatic pipes, and the heater were obtained from the steady-state form of Eqs. (1c), (2) and (5), and their expressions are Eqs. (18a) to (18c) respectively.

$$T^0_{f_j}(s_j) = T_c + b_j \cdot e^{-\beta_j(s_j - L)}\Delta T^0 \quad \text{cooler} \tag{18a}$$

$$T^0_{f_j}(s_j) = T^0_f(L) \quad \text{adiabatic pipe} \tag{18b}$$

$$T^0_{f_j}(s_j) = T^0_f(L) + \Delta T^0 \cdot \frac{s_j - L}{L_H} \quad \text{heater} \tag{18c}$$

Generalizing for the cooler, adiabatic pipe and heater, the inlet of each pipe is placed at a generic coordinate $s_j = L$, while $T^0_f(L)$ is the fluid temperature at the inlet of the pipe considered. Considering the two sides of the heat exchanger, naming $T_{f_1}(0)$ the inlet fluid temperature on the primary side and $T_{f_2}(0)$ the outlet fluid temperature of the heat exchanger secondary side, the temperature profiles obtained are represented in Eq. (19a) for the primary side of the heat exchanger and in Eq. (19b) for the secondary side. The equations are obtained from the steady-state form of Eqs. (5), (8), (10) and (11).

$$T^0_{f_1}(s_1) = T^0_{f_1}(0) + a \cdot (1 - e^{-\alpha s_1})\Delta T^0 \tag{19a}$$

$$T^0_{f_2}(s_2) = T^0_{f_2}(0) + \frac{\Gamma_1 c_{f_1}}{\Gamma_2 c_{f_2}} a \cdot \left[1 - e^{-\alpha(L_{tot_2} - s_2)}\right]\Delta T^0 \tag{19b}$$

where L_{tot_2} is the total length of the eDYNASTY loop. The values of the constants a and b_j depend on the pipe configurations of the CNCLs. The exponents α and β_j have the following expressions:

$$\alpha = \frac{\Gamma_2 c_{f_2} - \Gamma_1 c_{f_1}}{\Gamma_1\Gamma_2 c_{f_1} c_{f_2}\tilde{R}^{th}_{HE}} \tag{20}$$

$$\beta_j = \frac{1}{\Gamma_j c_{f_j}\tilde{R}^{th}_{COOL_j}} \tag{21}$$

The two thermal resistances introduced in Eqs. (20) and (21), $\tilde{R}^{th}_{HE}$ and $\tilde{R}^{th}_{COOL_j}$, are respectively the thermal resistance between the two

Table 3
Adopted heat transfer correlations.

Correlation name	Correlation formula	Reynolds range	Prandtl range
Hausen	$3.66 + \frac{0.0668(D/L)RePr}{1+0.04[(D/L)RePr]^{0.67}}$	$3.6 \cdot 10^3 \leq Re \leq 9.05 \cdot 10^5$	$3 \cdot 10^{-3} \leq Pr \leq 5 \cdot 10^{-2}$
Analytic solution	$\frac{48}{11}$	Laminar	Fully developed conditions, uniform q''
Skupinski	$4.82 + 0.0185(RePr)^{0.827}$	Laminar	Thermal entry, uniform T_w
Gnielinski	$\frac{(f/8)(Re-1000)Pr}{1+12.7(f/8)^{0.5}(Pr^{0.67}-1)}$ $f = [0.79 \cdot log(Re) - 1.64]^{-2}$	$3 \cdot 10^3 \leq Re \leq 5 \cdot 10^6$	$0.5 \leq Pr \leq 2 \cdot 10^3$
Dittus–Boelter	$0.023 \cdot Re^{0.8} Pr^n$ $n = \begin{cases} 0.3 & \text{fluid being cooled} \\ 0.4 & \text{fluid being heated} \end{cases}$	$Re \geq 10^4$	$0.6 \leq Pr \leq 160$

fluids at the heat exchanger and the thermal resistance between the fluid of the jth loop and the outer cooler wall surface. Their expressions are shown in equations Eq. (22):

$$\tilde{R}^{th}_{HE} = \frac{1}{\pi D_{f_1} h_{1_{HE}}} + \tilde{s}\tilde{R}_{w_1} + \frac{1}{\pi D_{w_{o_1}} h_{HE}} \tag{22a}$$

$$\tilde{R}^{th}_{COOL_j} = \tilde{s}\tilde{R}_{w_j} + \frac{1}{\pi D_{f_j} h_{j_{COOL}}} \tag{22b}$$

The temperatures that both fluids assume at the origin of each curvilinear coordinate, $T^0_{f_1}(0)$ and $T^0_{f_2}(0)$, are coupled thanks to the relation Eq. (23), which is derivable from Eqs. (5), (8), (10) and (11).

$$T^0_{f_2}(0) = T^0_{f_1}(0) + Q\tilde{R}^{th}_{HE} a\alpha \tag{23}$$

To determine the coefficients a in Eq. (19) and b_j in Eq. (18a), and the temperatures $T^0_{f_1}(0)$ and $T^0_{f_2}(0)$ in Eq. (19), the continuity of the temperature field for each loop must be imposed.

4.2. Integral momentum equations

The global balance of the momentum for both loops can be obtained by applying a path integral to Eq. (1b), including also Eq. (7) for the eDYNASTY loop, belonging to each loop, obtaining integral momentum Eqs. (24a) and (24b) for the DYNASTY and eDYNASTY loop respectively:

$$\frac{1}{2}\lambda^0_1 \frac{(G^0_1)^2}{\rho^*_{f_1}} \frac{L_{tot_1}}{D_{f_1}} = -\oint_{loop_1} \rho^0_{f_1} g\hat{\mathbf{e}}_z \cdot \hat{\mathbf{e}}_s \tag{24a}$$

$$\frac{1}{2}\lambda^0_2 \frac{(G^0_2)^2}{\rho^*_{f_2}} \frac{L_{tot_2} - L_{HE}}{D_{f_2}} + \frac{1}{2}\lambda^0_{HE} \frac{(G^0_{HE})^2}{\rho^*_{f_2}} \epsilon L_{HE} = -\oint_{loop_2} \rho^0_{f_2} g\hat{\mathbf{e}}_z \cdot \hat{\mathbf{e}}_s \tag{24b}$$

The relations state the balance between the distributed friction pressure drop on the left hand of both equations and the pressure that rises from the Buoyancy force on the right hand of the equations. In the case of the presence of concentrated pressure losses, such as elbows temperature probes or mass-flow meters, the frictional pressure drop term must include them.

$$\Delta p_{fric_j} = \Delta p_{distrib_j} + \Delta p_{conc_j} \tag{25}$$

which must be balanced by the Buoyancy force. The concentrated pressure losses can be modelled as follows [15]:

$$\Delta p_{conc_j} = \frac{1}{2} \frac{(G^0_j)^2}{\rho^*_{f_j}} \sum_{n=1}^{N_j} K_{n_j} \tag{26}$$

where K_{n_j} is a constant that depends on the nth device that causes the concentrated pressure drop and N_j is the total number of devices that cause the concentrated pressure losses in the jth loop. The momentum balance equation and the energy balance equation are coupled thanks to the Boussinesq approximation, Eq. (27):

$$\rho_{f_j} = \rho^*_{f_j} + \left(\frac{\partial \rho_{f_j}}{\partial T_{f_j}}\right)_p (T_{f_j} - T^*_{f_j}) = \rho^*_{f_j}[1 - \beta_{f_j}(T_{f_j} - T^*_{f_j})] \quad \text{with} \quad \beta_{f_j} = -\frac{1}{\rho^*_{f_j}}\left(\frac{\partial \rho_{f_j}}{\partial T_{f_j}}\right)_p \tag{27}$$

where β_{f_j} is the thermal expansion coefficient for the jth fluid evaluated at the reference temperature $T^*_{f_j}$. Inserting Eq. (27) in Eq. (24), the general integral momentum Eq. (28) is obtained for a generic NCL:

$$\Delta p_{fric_j} = \rho^*_{f_j} g\beta_{f_j} \oint_{loop_j} T^0_{f_j} \hat{\mathbf{e}}_z \cdot \hat{\mathbf{e}}_s ds_j \tag{28}$$

It is possible to demonstrate that for each NCL, the relation Eq. (29) holds [5]:

$$\oint_{loop_j} T^0_{f_j} \hat{\mathbf{e}}_z \cdot \hat{\mathbf{e}}_s ds_j = \Delta T^0 \mathcal{L}_{eq_j} \tag{29}$$

where $\mathcal{L}_{eq_j}$ is the thermal barycentre between the heat source and the heat sink of the jth loop. Referring to Fig. 1 of the CNCLs analysed, the thermal barycentres of the two loops assume the following expression:

$$\mathcal{L}_{eq_1} = \left[\frac{L_2}{L_H} + a \cdot \left(1 - e^{-\alpha L_{HE}}\right) + \frac{L_3}{2L_H}\right] L_3 - L_1 a \cdot \left(1 - e^{-\alpha L_{HE}}\right) - \frac{a}{\alpha}(\alpha L_{HE} - 1 + e^{-\alpha L_{HE}}) \tag{30a}$$

$$\mathcal{L}_{eq_2} = (l_6 - l_4)\frac{\Gamma_1 c_{f_1}}{\Gamma_2 c_{f_2}} a \cdot \left(1 - e^{-\alpha L_{HE}}\right) + \frac{\Gamma_1 c_{f_1}}{\Gamma_2 c_{f_2}} \frac{a}{\alpha}(\alpha L_{HE} - 1 + e^{-\alpha L_{HE}}) \tag{30b}$$

For a CNCLs problem, once the temperature fields belonging to each loop are determined, Eq. (31) are the remaining equations to solve:

$$\Delta p_{fric_1} = \rho^*_{f_1} g\beta_{f_1} \Delta T^0 \mathcal{L}_{eq_1} \tag{31a}$$

$$\Delta p_{fric_2} = \rho^*_{f_2} g\beta_{f_2} \Delta T^0 \mathcal{L}_{eq_2} \tag{31b}$$

Thus, it is necessary to find those mass fluxes (G_1, G_2) that satisfy Eq. (31). Since Eqs. (31a) and (31b) are non-linear equations, a numerical optimization algorithm, namely the Broyden one with second Jacobian approximation, has been coded in Python using the optimization library `scipy.optimize.root(method='broyden2')` [16]. Such a method has the best performance among the others implemented in the same library.

5. Stability analysis

In this section, stability analysis of the steady-state solution is presented. The analysis was conducted by linearizing the dynamic equations for NCL in the proximity of a steady-state, applying the Perturbation theory [2,4,12]. From these linear equations obtained, it

Table 4
Validity range of the perturbation applied to the state variables, referring to Eq. (32).

State variable x	Lower bound c	Upper bound d
G_1	0	L_{tot_1}
G_2	0	$L_{tot_2} - L_{HE}$
G_{HE}	$L_{tot_2} - L_{HE}$	L_{tot_2}
T_{f_j}	0	L_{tot_j}
$T_{w_{i_j}}$	0	L_{tot_j}
$T_{w_{o_j}}$	0	L_{tot_j}

was possible to derive a Stability Map for the CNCLs, following the same procedure adopted by [12].

5.1. Linear dimensionless governing equations

Following a similar approach adopted by [2], the state of the CNCLs system, identified by the mass fluxes G_j and the temperatures T_{f_j}, $T_{w_{i_j}}$, $T_{w_{o_j}}$, is perturbed around a steady-state solution (G_j^0, $T_{f_j}^0$, $T_{w_{i_j}}^0$, $T_{w_{o_j}}^0$) under the assumption of small perturbation compared to the steady-state values. Assuming x a generic state variable, the perturbation assumption is the following:

$$\begin{aligned} &x \cong x^0(s_j) + \delta x(s_j,t) \quad \text{with} \\ &\delta x(s_j,t) \ll x^0(s_j) \quad \forall (s_j,t) \in [c,d] \times \mathbb{R}^+ \end{aligned} \tag{32}$$

where c and d are the lower and upper bounds of the validity range of the perturbation applied to the state variables for the system, whose values are reported in Table 4.

The same approach of Eq. (32) is applied regarding the heat transfer coefficients and the friction factors: as they are functions of the system state, a perturbation of the state implies a perturbation to the heat transfer coefficients and the friction factors (33).

$$h_{j_m} \cong h_{j_m}^0 + \delta h_{j_m} \tag{33a}$$

$$\lambda_j \cong \lambda_j^0 + \delta\lambda_j \tag{33b}$$

Assuming constant thermo-physical properties, the perturbations applied to the heat transfer coefficients and the friction factors in Eq. (33) depend only on perturbations of the mass flux; moreover, perturbations are linearized as written in Eq. (34), following the same approach adopted by [4].

$$\delta h_{j_m} \approx \left(\frac{\partial h_{j_m}}{\partial G_j}\right)_0 \delta G_j \qquad \text{with} \quad \left(\frac{\partial h_{j_m}}{\partial G_j}\right)_0 := \left(\frac{\partial h_{j_m}}{\partial G_j}\right)\Big|_{G_j=0} \tag{34a}$$

$$\delta\lambda_j \approx \left(\frac{\partial \lambda_j}{\partial G_j}\right)_0 \delta G_j \qquad \text{with} \quad \left(\frac{\partial \lambda_j}{\partial G_j}\right)_0 := \left(\frac{\partial \lambda_j}{\partial G_j}\right)\Big|_{G_j=0} \tag{34b}$$

The perturbed variables, Eqs. (32) and (33), are substituted in Eqs. (1), (2) and (5) to (8). In this way, the set of the linear time-dependent governing equations, Eq. (35), are obtained for the perturbed variable for each of the two loops:

$$\frac{\partial(\delta G_j)}{\partial s_j} = 0 \tag{35a}$$

$$\frac{\partial(\delta G_j)}{\partial t} = -\frac{\partial(\delta p_j)}{\partial s_j} - \left(\frac{\partial^2 p_j}{\partial G_j \partial s_j}\right)_{distrib} \delta G_j - \delta\rho_{f_j} g \hat{\mathbf{e}}_z \cdot \hat{\mathbf{e}}_s \tag{35b}$$

$$\begin{aligned} \rho_{f_j}^* c_{f_j} \frac{\partial\delta(T_{f_j})}{\partial t} + \delta G_j c_{f_j} \frac{dT_{f_j}^0}{ds_j} + G_j^0 c_{f_j} \frac{\partial\delta(T_{f_j})}{\partial s_j} = \\ - h_{j_m}^0 (\delta T_{f_j} - \delta T_{w_{i_j}}) \frac{\tilde{S}_{f_j}}{\tilde{V}_{f_j}} \\ - \left(\frac{\partial h_{j_m}}{\partial G_j}\right)_0 \delta G_j (T_{f_j}^0 - T_{w_{i_j}}^0) \frac{\tilde{S}_{f_j}}{\tilde{V}_{f_j}} \end{aligned} \tag{35c}$$

$$\begin{aligned} \rho_{w_j} c_{w_j} \frac{\partial(\delta T_{w_{i_j}})}{\partial t} = h_{j_m}^0 (\delta T_{f_j} - \delta T_{w_{i_j}}) \frac{\tilde{S}_{f_j}}{\tilde{V}_{w_{i_j}}} \\ + \left(\frac{\partial h_{j_m}}{\partial G_j}\right)_0 \delta G_j (T_{f_j}^0 - T_{w_{i_j}}^0) \frac{\tilde{S}_{f_j}}{\tilde{V}_{w_{i_j}}} \\ - \frac{\delta T_{w_{i_j}} - \delta T_{w_{o_j}}}{\tilde{V}_{w_{i_j}} \tilde{R}_{w_j}} \end{aligned} \tag{35d}$$

$$\begin{cases} \delta T_{w_{o_j}} = 0 & \text{cooler} \\ \rho_{w_1} c_{w_1} \dfrac{\partial(\delta T_{w_{o_1}})}{\partial t} = \dfrac{\delta T_{w_{i_1}} - \delta T_{w_{o_1}}}{\tilde{V}_{w_{o_1}} \tilde{R}_{w_1}} & \\ \quad + h_{HE}^0 (\delta T_{f_2} - \delta T_{w_{o_1}}) \dfrac{\tilde{S}_{w_{o_1}}}{\tilde{V}_{w_{o_1}}} & \text{1st side HE} \\ \quad + \left(\dfrac{\partial h_{HE}}{\partial G_{HE}}\right)_0 \delta G_{HE} (T_{f_2}^0 - T_{w_{o_1}}^0) \dfrac{\tilde{S}_{w_{o_1}}}{\tilde{V}_{w_{o_1}}} & \\ \rho_{w_j} c_{w_j} \dfrac{\partial(\delta T_{w_{o_j}})}{\partial t} = \dfrac{\delta T_{w_{i_j}} - \delta T_{w_{o_j}}}{\tilde{V}_{w_{o_j}} \tilde{R}_{w_j}} & \text{o/w} \end{cases} \tag{35e}$$

where:

$$\left(\frac{\partial^2 p_j}{\partial G_j \partial s_j}\right)_{distrib} = \left[\frac{1}{2}\left(\frac{\partial \lambda_j}{\partial G_j}\right)_0 G_j^0 + \lambda_j^0\right] \frac{G_j^0}{\rho_{f_j}^*} \frac{1}{D_{f_j}} \tag{36}$$

The term (36) expresses the variation of the distributed pressure losses, per unit of pipe length, due to a variation of the mass flux in the same loop and it is valid also for the secondary side of the heat exchanger when the term $\frac{1}{D_{f_j}}$ is replaced with ϵ. Eq. (35) are valid for the secondary side of the heat exchanger, the only difference is in the fluid energy Eq. (35c): at the heat exchanger, it must be included the perturbation of the heat transfer between the secondary fluid and the outer wall surface of the primary loop. The momentum Eq. (35b) can be written in integral form, and thanks to Eq. (12), Eqs. (37a) and (37b) are obtained for the DYNASTY and eDYNASTY loop respectively.

$$\begin{aligned} \frac{d(\delta G_1)}{dt} L_{tot_1} = -\left(\frac{\partial p_1}{\partial G_1}\right)_{fric} \delta G_1 \\ - \rho_{f_1}^* g \beta_{f_1} \oint_{loop_1} \delta T_{f_1} \hat{\mathbf{e}}_z \cdot \hat{\mathbf{e}}_s ds_1 \end{aligned} \tag{37a}$$

$$\begin{aligned} \frac{d(\delta G_2)}{dt}\left[L_{tot_2} + \left(\frac{\tilde{V}_{f_2}}{\tilde{V}_{f_{HE}}} - 1\right) L_{HE}\right] = -\left(\frac{\partial p_2}{\partial G_2}\right)_{fric} \delta G_2 \\ - \rho_{f_2}^* g \beta_{f_2} \oint_{loop_2} \delta T_{f_2} \hat{\mathbf{e}}_z \cdot \hat{\mathbf{e}}_s ds_2 \end{aligned} \tag{37b}$$

where:

$$\left(\frac{\partial p_1}{\partial G_1}\right)_{fric} = \left(\frac{\partial^2 p_1}{\partial G_1 \partial s_1}\right)_{distrib} L_{tot_1} + \frac{G_1^0}{\rho_{f_1}^*} \sum_{n=1}^{N_1} K_{n_1} \tag{38a}$$

$$\begin{aligned} \left(\frac{\partial p_2}{\partial G_2}\right)_{fric} = \left(\frac{\partial^2 p_2}{\partial G_2 \partial s_2}\right)_{distrib} (L_{tot_2} - L_{HE}) \\ + \left(\frac{\partial^2 p_{HE}}{\partial G_{HE} \partial s_2}\right)_{distrib} \frac{\tilde{V}_{f_2}}{\tilde{V}_{f_{HE}}} L_{HE} + \frac{G_2^0}{\rho_{f_2}^*} \sum_{n=1}^{N_2} K_{n_2} \end{aligned} \tag{38b}$$

The above terms express the variation of the frictional pressure losses due to a variation in the mass flux for the DYNASTY loop, Eq. (38a), and for the eDYNASTY loop, Eq. (38b). The Laplace transform Eq. (39) was applied to the perturbed Eqs. (35) and (37).

$$\hat{f}(s_j,\omega) = \int_0^{+\infty} f(s_j,t) e^{-\omega t} dt \quad \text{with} \quad \omega \in \mathbb{C} \tag{39}$$

Eqs. (35) and (37) can be made dimensionless in order to obtain general equations which are suitable to any rectangular NCL of any dimension which adopts any fluid and any pipe materials. The following approximation was adopted for the infinitesimal volume of the inner and outer shell of the pipe wall:

$$\tilde{V}_{w_{o_j}} \approx \tilde{V}_{w_{i_j}} \approx \tilde{V}_{w_j} = \frac{\tilde{V}_{w_{o_j}} + \tilde{V}_{w_{i_j}}}{2}$$

The dimensionless linear equation of Eqs. (35) and (37) can be obtained by introducing the following dimensionless quantities:

$$\overline{\omega} = \omega \frac{L_{tot_1}\rho^*_{f_1}}{G^0_1} \quad \overline{G}_j = \frac{\hat{G}_j}{G^0_1} \quad \overline{T}_{f_j,w_{i_j},w_{o_j}} = \frac{\hat{T}_{f_j,w_{i_j},w_{o_j}}}{\Delta T^0}$$

$$\overline{\rho} = \frac{\rho^*_{f_2}}{\rho^*_{f_1}} \quad \overline{c} = \frac{c_{f_2}}{c_{f_1}} \quad \overline{\mu} = \frac{\mu_{f_2}}{\mu_{f_1}} \quad \overline{k} = \frac{k_{f_2}}{k_{f_1}} \quad \overline{\beta}_f = \frac{\beta_{f_2}}{\beta_{f_1}}$$

$$\overline{\rho}_{w_j} = \frac{\rho_{w_j}}{\rho^*_{f_1}} \quad \overline{c}_{w_j} = \frac{c_{w_j}}{c_{f_1}} \quad \overline{k}_{w_j} = \frac{k_{f_1}}{k_{w_j}}$$

$$\overline{s}_j = \frac{s_j}{L_{tot_1}} \quad \overline{L}_j = \frac{L_j}{L_{tot_1}} \quad \overline{l}_j = \frac{l_j}{L_{tot_1}} \quad \overline{\tau}_{w_j} = \frac{\tau_{w_j}}{L_{tot_1}}$$

$$\overline{S}_{f_j,w_{i_j},w_{o_j}} = \frac{\tilde{S}_{f_j,w_{i_j},w_{o_j}}}{L_{tot_1}} \quad \overline{V}_{f_j} = \frac{\tilde{V}_{f_j}}{L^2_{tot_1}} \quad \overline{V}_j = \frac{\tilde{V}_{f_1}}{\tilde{V}_{w_j}}$$

$$\overline{D}_{f_j,w_{i_j},w_{o_j}} = \frac{D_{f_j,w_{i_j},w_{o_j}}}{L_{tot_1}} \quad \overline{R}_{w_j} = \pi k_{w_j}\tilde{R}_{w_j}$$

$$\overline{\alpha} = \alpha \cdot L_{tot_1} \quad \overline{\beta}_j = \beta_j \cdot L_{tot_1} \quad \overline{\epsilon} = \epsilon \cdot L_{tot_1}$$

$$St^0_{m_{(j_m)}} = \frac{\overline{S}_{f_j}}{\overline{V}_{f_1}} \frac{Nu_{j_m}}{Re_j Pr_j} \quad B_{j_m} = \frac{Re_j}{Nu_{j_m}} \left(\frac{\partial Nu_{j_m}}{\partial Re_j}\right)$$

$$St^0_{m_{HE}} = \frac{\overline{S}_{w_{o_1}}}{\overline{V}_{f_1}} \frac{Nu_{HE}}{Re_2 Pr_2} \overline{D}_{f_2}\overline{\epsilon}$$

$$St^0_{m_{2_{HE}}} = \frac{\overline{S}_{w_{o_1}}}{\overline{V}_{f_1}} \frac{Nu_{2_{HE}}}{Re_2 Pr_2} \overline{D}_{f_2}\overline{\epsilon}$$

$$B_{HE} = \frac{Re_2}{Nu_{HE}} \left(\frac{\partial Nu_{HE}}{\partial Re_{HE}}\right) \frac{1}{\overline{D}_{f_2}\overline{\epsilon}}$$

$$\widetilde{\left(\frac{\partial p_j}{\partial G_j}\right)}_{fric} = \frac{L_{tot_1}\rho^*_{f_1}}{G^0_1}\left(\frac{\partial p_j}{\partial G_j}\right)_{fric} \quad \delta_{HE} = \frac{Re_2}{Re_1}\frac{D_{f_1}}{D_{f_2}}\overline{\mu}\,\overline{c}$$

$$\overline{\mathcal{L}}_{eq_j} = \frac{\mathcal{L}_{eq_j}}{L_{tot_1}} \quad \overline{\Delta p}_{fric_j} = \Delta p_{fric_j}\frac{\rho^*_{f_1}}{(G^0_1)^2}$$

where $Nu_{j_m} = Nu_m(Re_j, Pr_j)$, and the subscript m distinguishes the various correlations used in the cooler, heater, adiabatic pipe and heat exchanger zones. $St^0_{m_{(j_m)}}$ is the modified Stanton number [2] related to the Nu_{j_m} correlation. The dimensionless parameters $\overline{\rho}, \overline{c}, \overline{\mu}, \overline{k}, \overline{\beta}_f$ relate the thermo-physical properties of the fluid of the secondary loop with those of the primary one, while the variables $\overline{\rho}_{w_j}, \overline{c}_{w_j}, \overline{k}_{w_j}$ relate the thermo-physical properties of the pipe wall of the jth loop with those of the primary loop. Assuming constant thermo-physical properties, these parameters are fixed and do not depend on the system state. The dimensionless linear equations which derive thanks to the dimensionless parameters introduced are presented in Sections 5.1.1 and 5.1.2.

5.1.1. Momentum dimensionless perturbed equations

The integral linear dimensionless perturbed equations describing the momentum balance for both loops are Eqs. (40a) and (40b):

$$\left[\overline{\omega} + \widetilde{\left(\frac{\partial p_1}{\partial G_1}\right)}_{fric}\right]\overline{G}_1 = \frac{\overline{\Delta p}_{fric_1}}{\overline{\mathcal{L}}_{eq_1}} \oint_{loop_1} \overline{T}_{f_1}\,\hat{\mathbf{e}}_z \cdot \hat{\mathbf{e}}_s d\overline{s}_1 \tag{40a}$$

$$\left\{\left[\overline{L}_{tot_2} + \left(\frac{\overline{V}_{f_2}}{\overline{V}_{f_{HE}}} - 1\right)\overline{L}_{HE}\right]\overline{\omega} + \widetilde{\left(\frac{\partial p_2}{\partial G_2}\right)}_{fric}\right\}\overline{G}_2 = \frac{\overline{\Delta p}_{fric_2}}{\overline{\mathcal{L}}_{eq_2}} \oint_{loop_2} \overline{T}_{f_2}\hat{\mathbf{e}}_z \cdot \hat{\mathbf{e}}_s d\overline{s}_2 \tag{40b}$$

where relations (31) were implemented. The knowledge of the two functions $(\overline{T}_{f_1}, \overline{T}_{f_2})$ is necessary to compute the two integrals, and their expressions can be obtained from the energy perturbed equations.

5.1.2. Energy dimensionless perturbed equations

The perturbed linear dimensionless energy equations obtained for the DYNASTY loop, including the primary side of the heat exchanger, are Eqs. (41):

$$\overline{\omega}\overline{T}_{f_1} + \frac{d\overline{T}_{f_1}}{d\overline{s}_1} + \overline{G}_1\frac{1}{\Delta T^0}\frac{dT^0_{f_1}}{d\overline{s}_1} = -St^0_{m_{(1_m)}}(\overline{T}_{f_1} - \overline{T}_{w_{i,1}}) - B_{1_m}St^0_{m_{(1_m)}}\frac{T^0_{f_1} - T^0_{w_{i_1}}}{\Delta T^0}\overline{G}_1 \tag{41a}$$

$$\overline{\rho}_{w_1}\overline{c}_{w_1}\overline{\omega}\overline{T}_{w_{i,1}} = St^0_{m_{(1_m)}}\overline{V}_1(\overline{T}_{f_1} - \overline{T}_{w_{i,1}}) + B_{1_m}St^0_{m_{(1_m)}}\overline{V}_1\frac{T^0_{f_1} - T^0_{w_{i_1}}}{\Delta T^0}\overline{G}_1 - St^0_{m_{(1_m)}}\overline{V}_1\frac{\overline{T}_{w_{i,1}} - \overline{T}_{w_{o,1}}}{Nu_{1_m}\overline{k}_{w_1}\overline{R}_{w_1}} \tag{41b}$$

$$\begin{cases} \overline{T}_{w_{o,1}} = 0 & \text{cooler} \\ \overline{\rho}_{w_1}\overline{c}_{w_1}\overline{\omega}\overline{T}_{w_{o,1}} = St^0_{m_{(1_{HE})}}\overline{V}_1\frac{\overline{T}_{w_{i,1}} - \overline{T}_{w_{o,1}}}{Nu_{1_{HE}}\overline{k}_{w_1}\overline{R}_{w_1}} + St^0_{m_{HE}}\delta_{HE}\overline{V}_1(\overline{T}_{f_2} - \overline{T}_{w_{o,1}}) + B_{HE}St^0_{m_{HE}}\overline{c}\overline{V}_1\frac{T^0_{f_2} - T^0_{w_{o_1}}}{\Delta T^0}\overline{G}_{HE} & \text{1st side HE} \\ \overline{\rho}_{w_1}\overline{c}_{w_1}\overline{\omega}\overline{T}_{w_{o,1}} = St^0_{m_{(1_m)}}\overline{V}_1\frac{\overline{T}_{w_{i,1}} - \overline{T}_{w_{o,1}}}{Nu_{1_m}\overline{k}_{w_1}\overline{R}_{w_1}} & \text{o/w} \end{cases} \tag{41c}$$

where the subscript m in the heat transfer coefficient refers to the different zones of the cooler ($m = COOL$), heater ($m = H$), adiabatic pipe ($m = P$), and heat exchanger ($m = HE$). Eq. (42), regard the secondary loop linear dimensionless perturbed energy equations, but are not valid for the secondary side of the heat exchanger.

$$\overline{\rho}\,\overline{c}\,\overline{\omega}\overline{T}_{f_2} + \delta_{HE}\frac{d\overline{T}_{f_2}}{d\overline{s}_2} + \overline{c}\overline{G}_2\frac{1}{\Delta T^0}\frac{dT^0_{f_2}}{d\overline{s}_2} = -St^0_{m_{(2_m)}}\delta_{HE}\frac{\overline{V}_{f_1}}{\overline{V}_{f_2}}(\overline{T}_{f_2} - \overline{T}_{w_{i,2}}) - B_{2_m}St^0_{m_{(2_m)}}\overline{c}\frac{T^0_{f_2} - T^0_{w_{i_2}}}{\Delta T^0}\overline{G}_2 \tag{42a}$$

$$\overline{\rho}_{w_2}\overline{c}_{w_2}\overline{\omega}\overline{T}_{w_{i,2}} = St^0_{m_{(2_m)}}\delta_{HE}\overline{V}_2(\overline{T}_{f_2} - \overline{T}_{w_{i,2}}) + B_{2_m}St^0_{m_{(2_m)}}\overline{c}\overline{V}_2\frac{T^0_{f_2} - T^0_{w_{i_2}}}{\Delta T^0}\overline{G}_2 - St^0_{m_{(2_m)}}\delta_{HE}\overline{V}_2\frac{\overline{T}_{w_{i,2}} - \overline{T}_{w_{o,2}}}{Nu_{2_m}\overline{k}_{f_2}\overline{R}_{w_2}} \tag{42b}$$

$$\begin{cases} \overline{T}_{w_{o,2}} = 0 & \text{cooler} \\ \overline{\rho}_{w_2}\overline{c}_{w_2}\overline{\omega}\overline{T}_{w_{o,2}} = St^0_{m_{(2_m)}}\delta_{HE}\overline{V}_2\frac{\overline{T}_{w_{i,2}} - \overline{T}_{w_{o,2}}}{Nu_{2_m}\overline{k}_{f_2}\overline{R}_{w_2}} & \text{o/w} \end{cases} \tag{42c}$$

where the subscript m in the heat transfer coefficient refers to the different zones of the cooler ($m = COOL$), and adiabatic pipe ($m = P$). Regarding the secondary side of the heat exchanger, the following linear dimensionless energy Eqs. (43) were obtained:

$$\overline{\rho}\,\overline{c}\,\overline{\omega}\overline{T}_{f_2} + \delta_{HE}\frac{\overline{V}_{f_2}}{\overline{V}_{f_{HE}}}\frac{d\overline{T}_{f_2}}{d\overline{s}_2} + \overline{c}\overline{G}_{HE}\frac{1}{\Delta T^0}\frac{dT^0_{f_2}}{d\overline{s}_2} = -St^0_{m_{HE}}\delta_{HE}\frac{\overline{V}_{f_1}}{\overline{V}_{f_{HE}}}(\overline{T}_{f_2} - \overline{T}_{w_{o,1}}) - B_{HE}St^0_{m_{HE}}\overline{c}\frac{\overline{V}_{f_1}}{\overline{V}_{f_{HE}}}\frac{T^0_{f_2} - T^0_{w_{o_1}}}{\Delta T^0}\overline{G}_{HE} - St^0_{m_{2_{HE}}}\delta_{HE}\frac{\overline{V}_{f_1}}{\overline{V}_{f_{HE}}}(\overline{T}_{f_2} - \overline{T}_{w_{i,2}}) \tag{43a}$$

$$\overline{\rho}_{w_2}\overline{c}_{w_2}\overline{\omega}\overline{T}_{w_{i,2}} = St^0_{m_{2_{HE}}}\delta_{HE}\overline{V}_{HE}(\overline{T}_{f_2} - \overline{T}_{w_{i,2}}) + B_{HE}St^0_{m_{HE}}\overline{c}\overline{V}_{HE}\frac{T^0_{f_2} - T^0_{w_{o_1}}}{\Delta T^0}\overline{G}_{HE} - St^0_{m_{2_{HE}}}\delta_{HE}\overline{V}_{HE}\frac{\overline{T}_{w_{i,2}} - \overline{T}_{w_{o,2}}}{Nu_{2_{HE}}\overline{k}_{w_2}\overline{R}_{w_{HE}}} \tag{43b}$$

$$\overline{\rho}_{w_2}\overline{c}_{w_2}\overline{\omega}\overline{T}_{w_{o,2}} = St^0_{m_{2_{HE}}}\delta_{HE}\overline{V}_{HE}\frac{\overline{T}_{w_{i,2}} - \overline{T}_{w_{o,2}}}{Nu_{2_{HE}}\overline{k}_{w_2}\overline{R}_{w_{HE}}} \tag{43c}$$

The temperature gradients $\frac{1}{\Delta T^0}\frac{dT^0_{f_j}}{d\overline{s}_j}$, reported in Eq. (44), can be computed from the steady-state temperature profiles obtained in Section 4.

$$\frac{1}{\Delta T^0}\frac{dT^0_{f_j}}{d\overline{s}_j} = \begin{cases} -b_j\overline{\beta}_j e^{-\overline{\beta}_j(\overline{s}_j-\overline{L})} & \text{cooler(s)} \\ \frac{1}{\overline{L}_H} & \text{heater} \\ a\overline{\alpha}e^{-\overline{\alpha}\overline{s}_1} & \text{1st side HE} \\ -\frac{\overline{V}_{f_1}}{\overline{V}_{f_2}}\frac{a\overline{\alpha}}{\delta_{HE}}e^{-\overline{\alpha}(\overline{L}_{tot_2}-\overline{s}_2)} & \text{2nd side HE} \\ 0 & \text{o/w} \end{cases} \tag{44}$$

Moreover, from Eqs. (1c) and (8) in steady-state form, the following general relations are obtained:

$$\frac{T^0_{f_j} - T^0_{w_{i_j}}}{\Delta T^0} = -\frac{1}{St^0_{m_{(j_m)}}}\frac{\overline{V}_{f_j}}{\overline{V}_{f_1}}\frac{1}{\Delta T^0}\frac{dT^0_{f_j}}{d\overline{s}_j} \tag{45}$$

$$\frac{T^0_{f_2} - T^0_{w_{o_1}}}{\Delta T^0} = -\frac{1}{St^0_{m_{HE}}}\frac{\overline{V}_{f_2}}{\overline{V}_{f_1}}\frac{1}{\Delta T^0}\frac{dT^0_{f_2}}{d\overline{s}_2} \tag{46}$$

Once the two fields $(\overline{T}_{f_1}, \overline{T}_{f_2})$ are derived, the two path integral in Eqs. (40a) and (40b) can be computed.

5.2. Stability map

The Stability Map for the CNCLs is obtained by determining the stability of each steady-state, following the same procedure applied in [12]. As the problem was formulated by means of dimensionless parameters, imposing a steady-state for the system is equivalent to fixing the Reynolds and Prandtl numbers for both fluids adopted in the CNCLs. Indeed Eqs. (40) to (43) can be solved once the parameters (Re_1, Pr_1, Re_2, Pr_2) have been fixed. As the system is coupled, these parameters cannot be arbitrarily chosen, but they are related: first of all, once the dimensionless parameters $\overline{\rho}, \overline{c}, \overline{k}, \overline{\beta}_f, \overline{\mu}$ are fixed, the relation (47) between the two Prandtl number holds.

$$Pr_2 = \frac{\overline{c}\,\overline{\mu}}{\overline{k}}Pr_1 \tag{47}$$

Regarding the relationship between the Reynolds numbers, it is necessary to find a function f that relates the Reynolds of the primary loop to the Reynolds of the secondary loop:

$$f : Re_1 \longrightarrow Re_2$$

Taking the ratio between Eqs. (31a) and (31b), it is possible to obtain the function (48):

$$f(Re_1, Re_2, Pr_1, Pr_2) := \frac{\overline{\Delta p}_{fric_2}}{\overline{\Delta p}_{fric_1}} - \overline{\rho}\overline{\beta}_f\frac{\overline{\mathcal{L}}_{eq_2}}{\overline{\mathcal{L}}_{eq_1}} \tag{48}$$

The zeroes of the function Eq. (48) are the steady-states which are solutions of the CNCLs problem. In this way, by fixing the Reynolds and Prandtl numbers of the primary fluid (Re_1, Pr_1), the Reynolds and Prandtl numbers of the secondary fluid (Re_2, Pr_2) can be obtained by solving the non-linear system of equations, Eq. (49):

$$\begin{cases} Pr_2 = \frac{\overline{c}\,\overline{\mu}}{\overline{k}}Pr_1 \\ f(Re_1, Re_2, Pr_1, Pr_2) = 0 \end{cases} \tag{49}$$

Once the steady-state is obtained by solving the system of Eqs. (49), its stability can be determined by searching all the poles $\overline{\omega}^*$ which are solutions of Eq. (40). In the case any of these complex poles has a positive real part ($\Re\mathfrak{e}\{\overline{\omega}^*\} > 0$), then the system is unstable, otherwise it is stable [17]. This is the same procedure adopted by [12] to obtain Stability Maps for the SCNL configurations, where it had only been necessary to find the poles of the equation of the DYNASTY loop (40a). In the CNCLs case, the problem is that a system of two equations must be solved, Eq. (40), but the variables are three: $\overline{\omega}, \overline{G}_1, \overline{G}_2$. To cope with this issue, Eq. (40) was modified dividing each of them by the term $\overline{G}_1$:

$$\overline{\omega} + \widetilde{\left(\frac{\partial p_1}{\partial G_1}\right)}_{fric} = \frac{\overline{\Delta p}_{fric_1}}{\overline{\mathcal{L}}_{eq_1}}\oint_{loop_1}\frac{\overline{T}_{f_1}}{\overline{G}_1}\hat{\mathbf{e}}_z\cdot\hat{\mathbf{e}}_s d\overline{s}_1 \tag{50a}$$

$$\left\{\left[\overline{L}_{tot_2} + \left(\frac{\overline{V}_{f_2}}{\overline{V}_{f_{HE}}} - 1\right)\overline{L}_{HE}\right]\overline{\omega} + \widetilde{\left(\frac{\partial p_2}{\partial G_2}\right)}_{fric}\right\}\frac{\overline{G}_2}{\overline{G}_1} = \frac{\overline{\Delta p}_{fric_2}}{\overline{\mathcal{L}}_{eq_2}}\oint_{loop_2}\frac{\overline{T}_{f_2}}{\overline{G}_1}\hat{\mathbf{e}}_z\cdot\hat{\mathbf{e}}_s d\overline{s}_2 \tag{50b}$$

In this way, the two integrals Eqs. (50a) and (50b) are functions of the two variables $\left(\overline{\omega}, \frac{\overline{G}_2}{\overline{G}_1}\right)$, obtaining a set of two equations in two variables, thus the problem is determined. As Eqs. (50a) and (50b) are non-linear functions of the complex variable $\overline{\omega}$, the poles can be obtained only by implementing a numerical optimization algorithm, as it is impossible to get an analytical solution. Following the same procedure adopted by [2,12] the Trust-Region-Dogleg algorithm [18], which is present in the [19] libraries, could be implemented. Thus, the stability/instability of a specific steady-state, identified by the vector state (Re_1, Re_2, Pr_1, Pr_2), can be analysed by imposing the Reynolds and Prandtl numbers of the primary loop, which represents its own steady-state (Re_1, Pr_1). The steady-state of the secondary loop (Re_2, Pr_2) is then derived through Eqs. (47) and (48). Once the steady-state of the CNCL is fixed, its stability is determined by analysing the real part of the poles of the system $\overline{\omega}$ obtained through Eq. (50). The flowchart of the algorithm adopted for determining the stability of each steady-state of the CNCL is shown in Fig. 4.

One consideration on the numerical resolution of Eq. (50) is that the algorithm requires two initial guesses in order to converge to a solution $\left(\overline{\omega}, \frac{\overline{G}_2}{\overline{G}_1}\right)^*$: one guess for the complex frequency $\overline{\omega}$ and another guess for the mass flux ratio $\frac{\overline{G}_2}{\overline{G}_1}$ respectively. It is expected that the mass flux ratio $\left(\frac{\overline{G}_2}{\overline{G}_1}\right)^*$, solution of Eq. (50), could be more than one and for each $\left(\frac{\overline{G}_2}{\overline{G}_1}\right)^*$ the ensemble of poles $\overline{\omega}^*$ can changes. For determining the stability of the system only the knowledge of the poles values is required, so the parameter $\frac{\overline{G}_2}{\overline{G}_1}$ can be seen as an extra variable, and reducing the problem solving of the set of equations, Eq. (50), to only one equation, which depends on the complex frequency, would simplify the issue. One strategy could be to express the mass flux ratio $\frac{\overline{G}_2}{\overline{G}_1}$ as a function of the complex frequency $\overline{\omega}$, and replacing the found relation in one of Eqs. (50a) and (50b) decreases to one the number of variables.

It is possible to extract the function between the complex frequency and the mass flux ratio through the momentum balance of the primary loop by Eq. (50a), as it is possible to write:

$$\oint_{loop_1}\frac{\overline{T}_{f_1}}{\overline{G}_1}\hat{\mathbf{e}}_z\cdot\hat{\mathbf{e}}_s d\overline{s}_1 = F_1(\overline{\omega}) + F_2(\overline{\omega})\frac{\overline{G}_2}{\overline{G}_1} \tag{51}$$

In this way, from Eq. (50a), a result which form can be expressed as Eq. (52) was obtained.

$$\frac{\overline{G}_2}{\overline{G}_1} = \frac{\left[\overline{\omega} + \widetilde{\left(\frac{\partial p_1}{\partial G_1}\right)}_{fric}\right]\frac{\overline{\mathcal{L}}_{eq_1}}{\overline{\Delta p}_{fric_1}} - F_1(\overline{\omega})}{F_2(\overline{\omega})} \tag{52}$$

Substituting this result in Eq. (50b), a unique nonlinear equation in one variable is obtained, which can be solved with the Trust-Region-Dogleg algorithm. The Stability Map for CNCLs was obtained assuming adiabatic the cooler of the DYNASTY loop, the same fluids in both loops ($\overline{\rho} = 1, \overline{c} = 1, \overline{k} = 1, \overline{\beta}_f = 1, \overline{\mu} = 1$) and the same wall parameters adopted

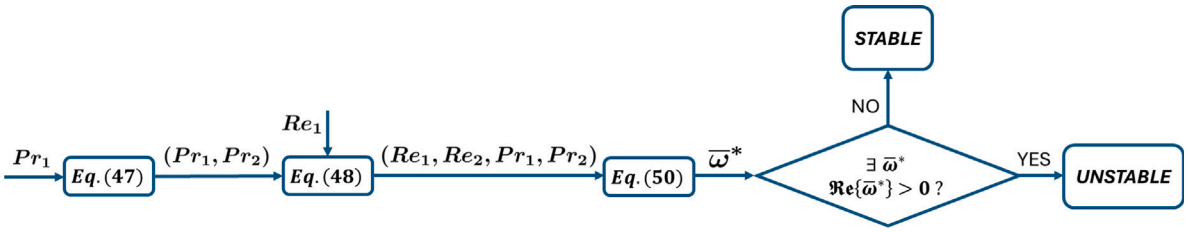

Fig. 4. Flowchart of the algorithm adopted for determining the stability of a steady-state, implemented in [19] to derive the Stability Map of the CNCL. In this algorithm, only two variables (Re_1, Pr_1) are needed as inputs to determine the stability of the system.

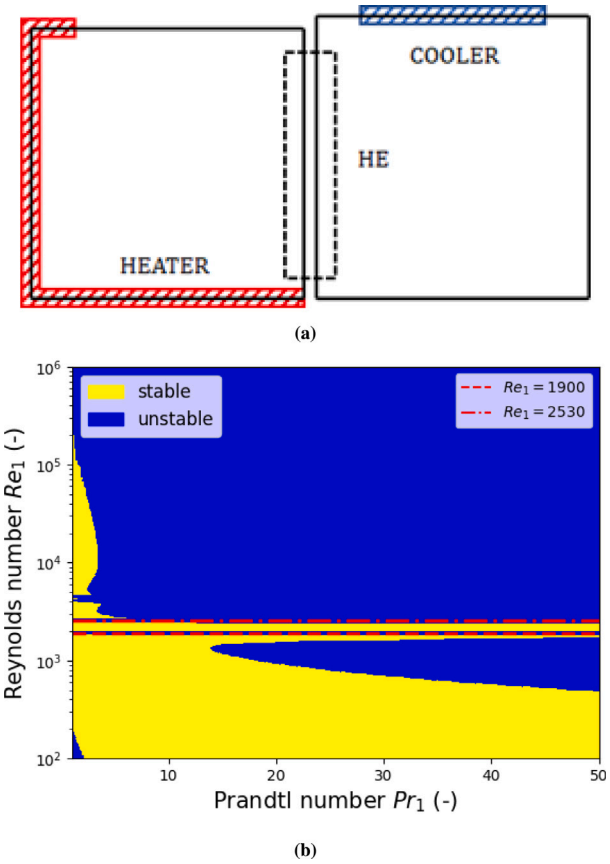

Fig. 5. (a) CNCLs configuration studied and its (b) Stability Map expressed as function of the Reynolds and Prandtl number of the primary loop (Re_1, Pr_1). In Fig. 5(b) the red dashed lines refers to the transition regime for the primary loop $(Re_1 = 2530)$ and the secondary loop $(Re_1 = 1900)$, this last value reported as value of primary Reynolds number thanks to Eq. (48).

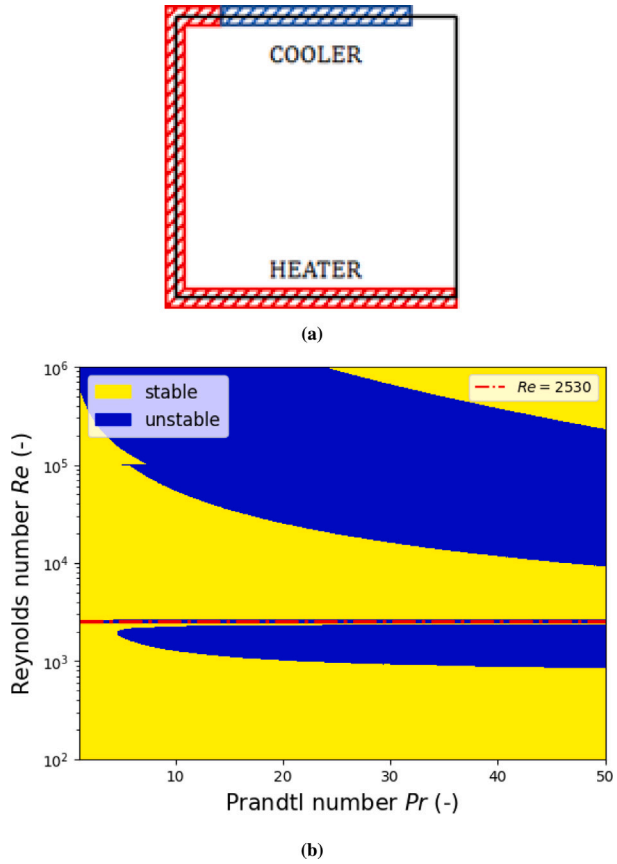

Fig. 6. (a) SCNL configuration adopted for the comparison and its (b) Stability Map expressed as function of the Reynolds and Prandtl number of the loop (Re, Pr). The red dashed line refers to the transition regime fixd at $(Re = 2530)$.

by [12] for determining the Stability Maps for SCNL configurations: $\overline{\rho}_{w_j} = 8.33$, $\overline{c}_{w_j} = 0.1119$, and $\overline{k}_{w_j} = 0.04$. Moreover, concentrated pressure losses were not considered.

Fig. 5 shows the Stability Map for the CNCLs as a function of Reynolds and Prandtl numbers of the primary fluid. The non-linear phenomenon of the natural circulation has been linearized in order to obtain Stability Map for predicting the stability or instability of the steady-states for a CNCLs. The aim is to study the behaviour of a non-linear phenomenon through an approximated model. With a similar procedure, the same adopted by [2], the Stability Map of the SCNL configuration, which is shown in Fig. 6, was obtained.

In order to investigate the effects of different cooling systems adopted for the primary loop in EHS configuration, the two Stability Maps (Figs. 5(b) and 6(b)) have been compared. It is possible to notice that the additional thermal inertia to the primary loop, given by the second loop, has a twofold effect: it stabilizes the system for laminar flow regime ($Re \lesssim 2530$) but it increases the unstable zone for turbulent flow regime. A reason for this latter phenomenon can be caused by feedback that characterizes the dynamics inside the heat exchanger. It could be that during a transient phenomenon, the primary mass flux (G_1) increases by a fluid temperature increasing. In this case, more heat is exchanged with the secondary side due to a hotter primary fluid. In the secondary loop, the fluid heats up and the mass flux (G_2) increases, increasing at the same time the efficiency of the heat transfer. This causes a cooling of the primary fluid, and consequently a decrease in the primary mass rate which worsens the heat transfer. Then, less heat is absorbed by the secondary loop, where the temperature and the mass rate decrease. At this point, the primary loop can no longer transfer the whole thermal power, causing an increase in the primary temperature and mass rate, restarting the process. The friction pressure losses are not able to dampen these effects and an oscillatory behaviour is established.

In Fig. 5(b), there are two zones in the region of the Reynolds number between 1000 and 10 000 where the system is unstable for

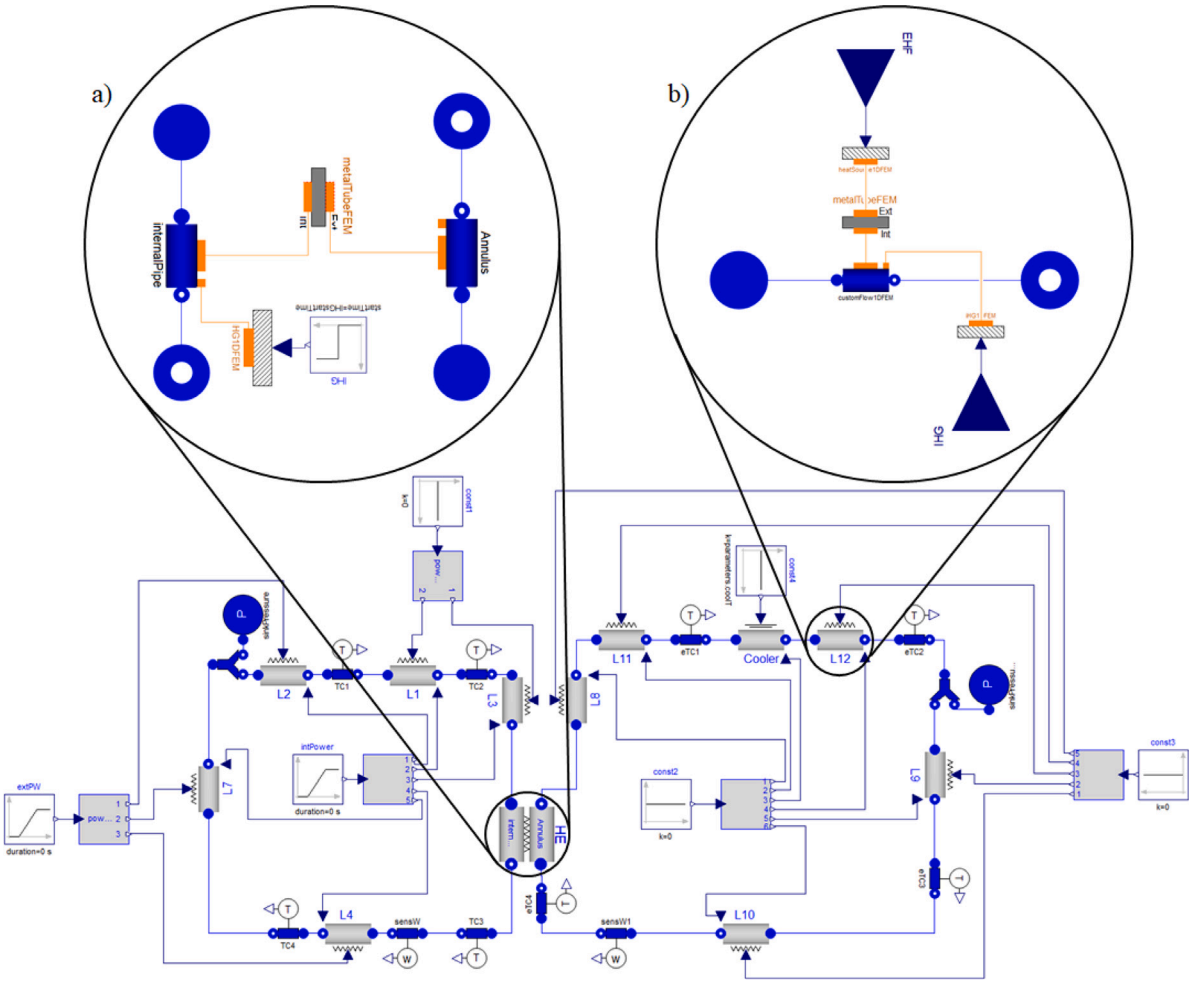

Fig. 7. Scheme of the MODELICA model adopted for the CNCLs simulations, showing the detailed models for the (a) heat exchanger and (b) a pipe. The pipe model (b) was adopted for all the pipes of both loops, specifying the imposed heat flux (q'') for the heater zone and the adiabatic pipes, or the imposed temperature for the cooler (T_c) at the connector EHF. The objects named TC and eTC are referred to as the thermocouples of the DYNASTY and eDYNASTY loop respectively, and they allow to give information about the fluids' state such as temperature and pressure.
Source: Adapted from [6].

any Prandtl number of the fluid. The same phenomenon occurs in Fig. 6(b), but in this case only one unstable zone extends for any Prandtl number. These regions occurs at very specific Reynolds numbers: they are related to the Reynolds number for the transition from laminar to turbulent flow regime (Section 3.4). This fact justifies the reason for the unstable horizontal line at $Re = 2530$ in Fig. 6(b) for the SCNL. Regarding the CNCL, two loops compose the system under study, so the transition regime can occur in one of the two loops. In particular, when the first loop is in the transition regime, at $Re_1 = 2530$, the system is unstable in accordance with the SCNL case, justifying the unstable line at such Reynolds number in Fig. 5(b). When the transition regime occurs in the second loop, at $Re_2 = 2530$, more considerations are needed: clearly, at this Re, the loop itself is unstable; thanks to Eq. (48), it is possible to relate the Reynolds number of the two loops, discovering that, when the Reynolds number of the fluid in the secondary loop is around the transition regime, the Reynolds number of the fluid in the secondary loop is $Re_1 \approx 1900$, justifying the second unstable line in Fig. 5(b).

6. Reference model for verification

Verification and validation of any model are important procedures which must be performed to ensure the reliability and results accuracy of the model. Planning to organize an experimental campaign at the DYNASTY-eDYNASTY facility to validate the models of the steady-state and stability maps described in Sections 4 and 5, their verification has been performed by comparing the obtained results with those acquired from a 1D model of the facility developed the in MODELICA language and described in [8]. The simulation campaign performed with this model has shown a satisfactory and accurate prediction of the DYNASTY facility behaviour in the heating transient compared to experimental data, justifying the reason for choosing this model to verify the analytical ones. For completeness, a brief description of the MODELICA model is reported below, along with some results.

6.1. DYNASTY-eDYNASTY MODELICA model

DYMOLA® is an Integrated Development Environment (IDE) based on the simulation language MODELICA [20]. MODELICA allows the description of each component of a system (called object) through physical and engineering principles, such as energy and mass balance [21]. The objects are connected by connectors to describe the mass and energy exchange among the components, thus obtaining a complete model of the system. This approach allows to build highly flexible models, as each component can be substituted without the necessity of writing the model of the entire system from scratch [21]. The model developed for the NCLs uses an extended version of the *ThermoPower* library [22], called *ThermoPowerIHG*, [8]. The MODELICA

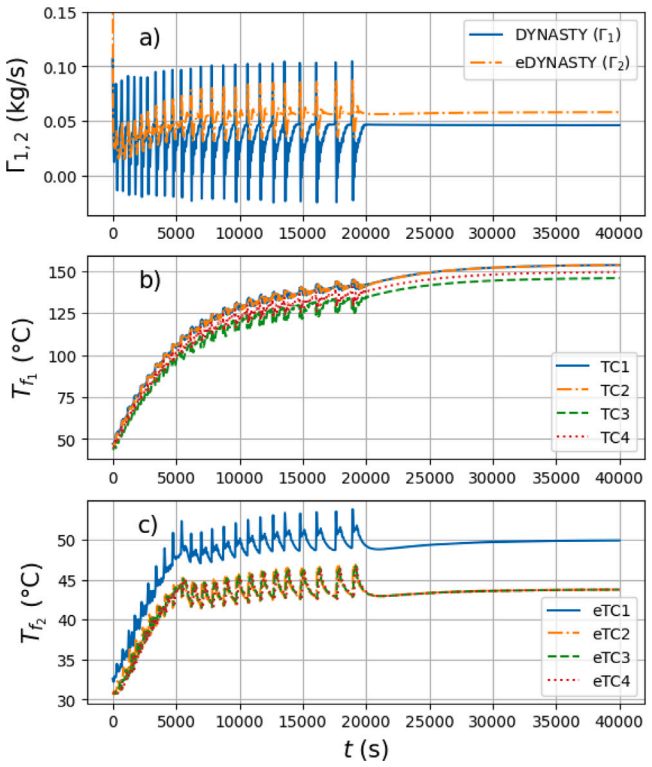

Fig. 8. Simulation results of a stable state performed with the MODELICA model of the CNCLs (Fig. 7) with $Pr = 5$ for both fluids, imposed power at the heater of the DYNASTY loop $Q = 1500$ W and imposed temperature of the cooler of the eDYNASTY loop $T_c = 25$ °C. Figure (a) shows the mass rates evolution in the DYNASTY and eDYNASTY loop, Figures (b) and (c) show the temperature evolution of the fluids in the DYNASTY and eDYNASTY loop respectively, keeping the notation for the thermocouples adopted in Fig. 7.

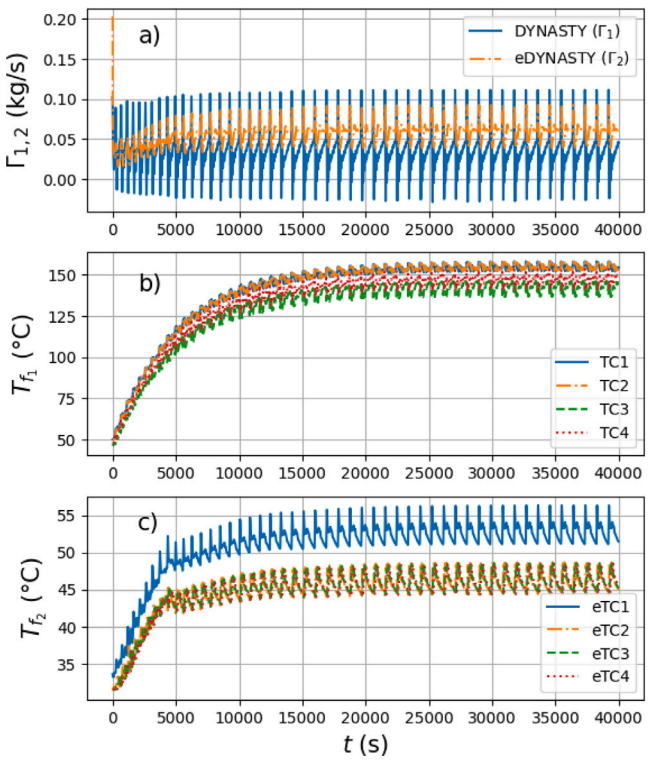

Fig. 9. Simulation results of an unstable state performed with the MODELICA model of the CNCLs (Fig. 7) with $Pr = 5$ for both fluids, imposed power at the heater of the DYNASTY loop $Q = 1700$ W and imposed temperature of the cooler of the eDYNASTY loop $T_c = 25$ °C. Figure (a) shows the mass rates evolution in the DYNASTY and eDYNASTY loop, Figures (b) and (c) show the temperature evolution of the fluids in the DYNASTY and eDYNASTY loop respectively, keeping the notation for the thermocouples adopted in Fig. 7.

model (Fig. 7) developed for the validation is a simplified version of the one developed by [6], where dissipation of the heat with the environment was not taken into account and a simpler model of the cooling system was implemented. Fig. 7 shows also the details of the models developed for the pipes and heat exchanger and adopted by [6]. Regarding the model of the heat exchanger in Fig. 7a, *internalPipe* and the *Annulus* are respectively the primary and secondary loop sections of the heat exchanger. The model for the cooler is similar to the pipe's one, with the difference of imposed temperature at the external pipe's wall instead of imposed heat flux (EHF connector in Fig. 7b). Each of these models adopts as a fluid model the *customFlow1DFEM* from the library *ThermoPowerIHG*, or its modification as for *Annulus* and *internalPipe* for the heat exchanger. To model the walls of the pipes, the *metalTubeFEM* was taken from library *ThermoPower*. To account for the motion of the fluid in the axial direction, the *ThermoPower* library uses a Finite Elements Methods (FEM) approach which is able to model flow inversion. MODELICA then simulates the time evolution of the model using different numerical integration algorithms. Following the results in [8] the one adopted to simulate the DYNASTY-eDYNASTY facility was the Radau2a algorithm [23]. The model, once the heat power and the external wall temperature at the cooler of the eDYNASTY loop are fixed (the one in the DYNASTY loop was assumed adiabatic, for consistency with the data obtained with the models developed in this paper), can simulate the transitory behaviour of the system, obtaining the time evolution of the quantities of interest, such as temperatures and mass rates, starting from initial conditions imposed. The fluids adopted for both the two loops were modelled assuming constant thermo-physical parameters, the same values as those adopted for the steady-state and stability analysis.

6.2. *DYNASTY-eDYNASTY model simulations*

The results of the analytical models developed in this work refer to the asymptotic behaviour for time $t \to +\infty$ of CNCLs systems. Therefore, it is necessary to understand when the stationarity or the instability of the system is reached in each DYMOLA® simulation; specifically, for verification purposes it is important to understand when the transient, caused by the initial condition, is extinguished.

By definition, a steady-state is characterized to have all the time derivatives equal to 0, meaning no time evolution. Thus, in any DYMOLA® simulation, if the state of the system, which is identified by the mass rates and temperatures, has reached a point in the graph space of state-time where the slope is flattened in time, then stationarity is reached. Moreover, such a steady-state can be also declared stable, as the initial state can be seen as a perturbation of the steady-state one, whose amplitude is dampened converging to the steady-state. Regarding unstable states, the mathematical definition provided by Lyapunov, which is the basis of the model developed to obtain Stability Maps, cannot be applied to unstable steady-states. Therefore, as explained by [12], a different stability definition was introduced: if a system reaches a steady state after a transient, such state is stable; otherwise it is in unstable equilibrium. Analytically, unstable states could also diverge indefinitely in time, but in these types of problems, it is not possible due to negative feedback which characterizes all these types of thermodynamic systems, as heat dissipations are a function of the state of the system due to the dependence of the heat transfer coefficients to the Reynolds and Prandtl number of the fluid [14]. For this reason, only limited instabilities are expected in NCLs problems. A method must be adopted to identify if the simulation of an apparently unstable state is effectively unstable or if it is a transient phenomenon,

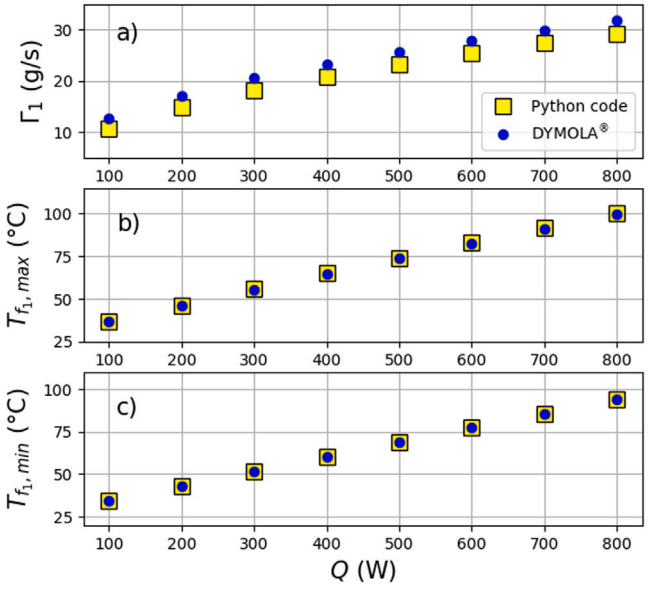

Fig. 10. Comparison of the steady-states obtained for the DYNASTY loop with the in-house code and DYMOLA® simulations of the MODELICA model (Fig. 7). The simulations were performed by imposing the temperature at the eDYNASTY cooler at $T_c = 25$ °C and varying the power at the heater Q at the DYNASTY loop. Figure (a) reports the mass rates, figure (b) the maximum temperatures and figure (c) the minimum temperature established in the DYNASTY loop respectively.

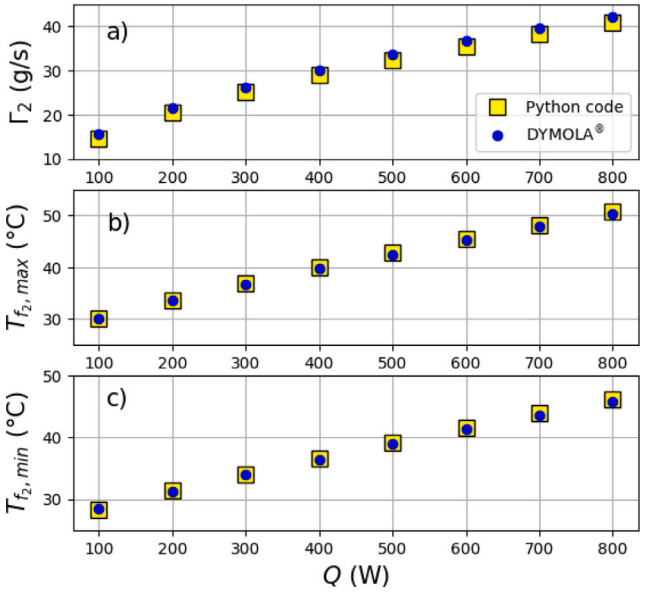

Fig. 11. Comparison of the steady-states obtained for the eDYNASTY loop with the in-house code and DYMOLA® simulations of the MODELICA model (Fig. 7). The simulations were performed by imposing the temperature at the eDYNASTY cooler at $T_c = 25$ °C and varying the power at the heater Q at the DYNASTY loop. Figure (a) reports the mass rates, figure (b) the maximum temperatures and figure (c) the minimum temperature established in the eDYNASTY loop respectively.

which then converges to a steady-state after a certain time. In all the cases simulated for the purpose of this paper, unstable states showed an oscillatory-like behaviour, as also in the cases simulated and studied by [2,12]. When the transitory behaviour is extinguished, if the state oscillates around an average state reaching a plateau, as in the case reported in Fig. 9, then it can be stated that such oscillatory behaviour continues indefinitely in time, and the state at such operative conditions is declared unstable.

Two examples of two simulations at different operative conditions, power at the heater 1.5 kW and 1.7 kW and wall temperature of the secondary cooler 25 °C, are reported to distinguish a stable state, Fig. 8, and unstable state, Fig. 9, with the Prandtl number $Pr_{1,2} = 5$ for both fluids. From the comparison of the two simulations, Figs. 8 and 9, it was noticed that even if both simulations had a similar initial trend of the system state, choosing a simulation time $t \lesssim 20\,000$ s would not be sufficient to declare the simulation stable or unstable also because the plateau had not yet been reached, justifying the method just described for determining the stability/instability of the simulation. In all the simulations performed by DYMOLA®, applying the criteria just presented, it was observed that a simulation time $t = 40\,000$ s was sufficient to declare stable or unstable the state under study.

7. Results and discussion

7.1. Steady-state verification

The steady-state solutions obtained through the developed in-house Python code were compared with the stable solutions obtained from the DYMOLA® simulations. Water was used as working fluid for both the DYNASTY and eDYNASTY loop, which constant thermo-physical properties were computed using the IF-97 standard water at a temperature of 25 °C and pressure 1 bar [24]. Concentrated pressure losses were not considered, as they were not included in the MODELICA model (Fig. 7), the cooler of the DYNASTY loop was assumed adiabatic, and the temperature imposed at the wall of the eDYNASTY cooler was 25 °C. The heat power imposed at the heater ranges from 100 W to 800 W, increasing the power of 100 W for each simulation. The mass

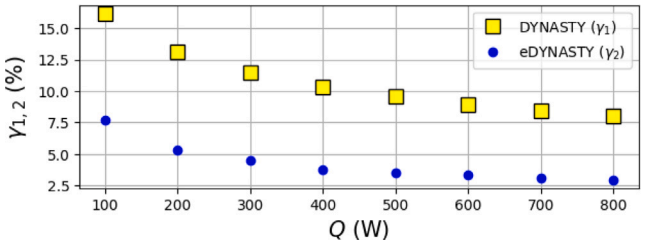

Fig. 12. Relative error, computed with Eq. (53), committed by the in-house code data with respect the DYMOLA® results regarding the mass rates plotted in Fig. 10a and Fig. 11a for the DYNASTY and eDYNASTY loop respectively.

rates, maximum and minimum temperatures were chosen to verify the results, in particular, Fig. 10 refers to the steady-states of the DYNASTY loop while Fig. 11 refers to the steady-states of the eDYNASTY loop. The DYMOLA® results were obtained by taking the values of the state assumed at the time $t = 40\,000$ s. From the comparison of the results, Figs. 10 and 11, it is noticed that the in-house code is able to predict the temperatures for both the loops and the entire power range analysed with good accuracy. Regarding the mass rates, the in-house code tends to underestimate their values with respect to the DYMOLA® solutions, it was noticed that a mesh refinement of the MODELICA model does not influence its results to justify the gap, but the trends of the results of the two models by a power variation are similar. The relative error was computed starting from mass rates with Eq. (53).

$$\gamma_j = \frac{\Gamma_j^{DYM} - \Gamma_j^{Py}}{\Gamma_j^{DYM}} \cdot 100 \tag{53}$$

$\Gamma_j^{DYM}, \Gamma_j^{Py}$ are the mass rate results obtained from the DYMOLA® simulations and the Python code respectively and plotted in Fig. 10a for the DYNASTY loop and Fig. 11a for eDYNASTY loop. It was observed that the relative error committed by the in-house code solutions was not higher than $\approx 16\%$ for low heat power, and its absolute value decreases with the power increasing, as Fig. 12 shows.

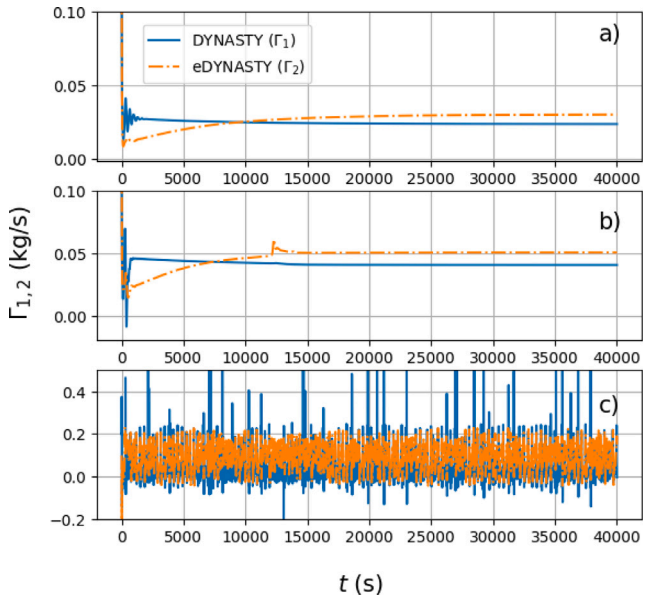

Fig. 13. Mass rates of the DYNASTY and eDYNASTY loop obtained through DYMOLA® simulation with $Pr = 5$ for both fluid, an imposed temperature at the eDYNASTY cooler of $T_c = 25$ °C and a power at the heater of (a) $Q = 0.3$ kW, (b) $Q = 1$ kW, (c) $Q = 9$ kW respectively (Table 5).

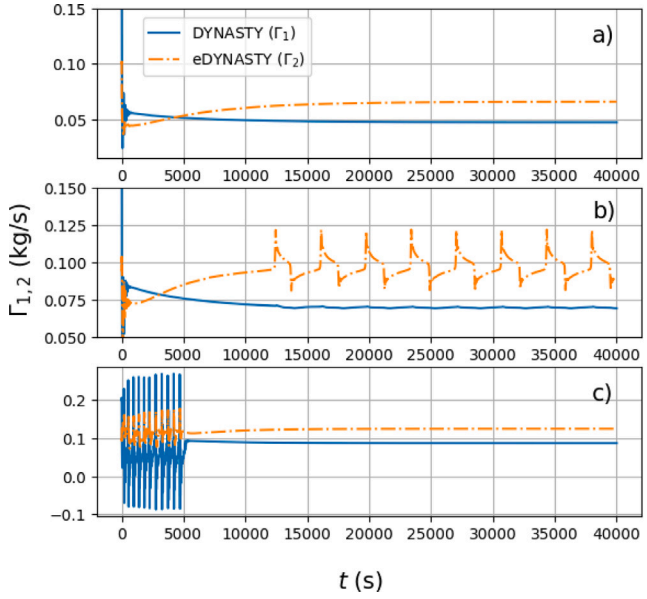

Fig. 14. Mass rates of the DYNASTY and eDYNASTY loop obtained through DYMOLA® simulation with $Pr = 10$ for both fluid, an imposed temperature at the eDYNASTY cooler of $T_c = 25$ °C and a power at the heater of (a) $Q = 3$ kW, (b) $Q = 7.5$ kW, (c) $Q = 15$ kW respectively (Table 6).

A possible explanation for the mass rate difference could be attributed to the different formulations adopted for the energy equation: in this work, it has been adopted an energetic approach, while in the MODELICA model, the *ThermoPowerIHG* library adopts an enthalpic formulation.

7.2. Stability map verification

A preliminary verification of the Stability Map obtained for the CNCLs system, Fig. 5, has been conducted by selecting some points of the map, through the help of the in-house code developed, and observing the behaviour of the DYMOLA® simulations at the same operative conditions of the points under study. Initially, fluids were selected for both loops for the in-house code and MODELICA model to be consistent with the dimensionless parameters introduced in Section 5.1 and fixed in Section 5.2 to obtain the Stability Map (Fig. 5). Regarding the in-house code, the thermo-physical properties of the fluid of the DYNASTY loop were chosen in order to satisfy the dimensionless wall thermo-physical properties ($\overline{\rho}_{w_j} = 8.33$, $\overline{c}_{w_j} = 0.1119$, $\overline{k}_{w_j} = 0.04$), as reported in Section 5.2, and the dimensional ones ($\rho_{w_j} = 8238$ kg/m^3, $c_{w_j} = 468$ J/(kg K), $k_{w_j} = 13.4$ W/(m K)), as reported in Section 3.1. Through these parameters fixed, it has been possible to compute the thermo-physical properties of the primary fluid (54).

$$\begin{aligned} \rho^*_{f_1} &= 988.95 \ \text{kg/m}^3 \\ c_{f_1} &= 4182.3 \ \text{J/(kg K)} \\ k_{f_1} &= 0.536 \ \text{W/(m K)} \end{aligned} \tag{54}$$

Moreover, to obtain the Stability Map (Fig. 5(b)) the following dimensionless parameters were fixed: $\overline{\rho} = 1, \overline{c} = 1, \overline{k} = 1, \overline{\beta}_f = 1, \overline{\mu}_f = 1$, as reported in Section 5.2. These parameters express the ratio between the thermo-physical properties of the secondary and primary fluid for the densities, specific heats, thermal conductivities, coefficients of thermal expansion and viscosities, relatively. Since the ratios are unitary, this means that the thermo-physical properties imposed for the secondary fluid ($\rho^*_{f_2}$, c_{f_2}, k_{f_2}) are identical to the primary ones (54). The remaining parameter to be fixed was the fluid viscosity (μ_{f_1}), which allowed to selection of the Prandtl number of the primary fluid (Pr_1), as the thermal capacity and thermal conductivity have just been selected (Eq. (54)). Once the thermo-physical properties of both fluids were selected, imposing the operational conditions, as heat power Q and imposed wall temperature of the eDYNASTY cooler T_c, to the in-house code, allows to compute the mass rates that are established in both loops, in this way, it is possible to compute the Reynolds numbers of the fluids. In summary, in order to select a point in the Stability Map (Fig. 5), once the dimensionless parameters used to obtain the Stability Map are in accordance with the thermo-physical properties of the wall and the fluids of the in-house code, the Prandtl number can be imposed by choosing the primary fluid's viscosity (μ_{f_1}), and the Reynolds numbers can be computed by imposing the operative conditions (Q, T_c) through the in-house code. The same fluids and wall parameters were imposed in the MODELICA model and the simulations have been conducted at the same operational conditions in order to verify if the points of the Stability Map (Fig. 5) can predict the stability or instability of the CNCLs. In this analysis, the cooler temperature was imposed at 25 °C and two Prandtl numbers were selected $Pr_1 = 5$ and $Pr_1 = 10$ (the Prandtl numbers of the secondary fluid Pr_2 were the same thanks to equation Eq. (47)). In this case, only the power has been allowed to vary in order to reach the desired Reynolds numbers. The cases studied are summarized in Table 5 for the fluid with $Pr_1 = 5$ and in Table 6 for the fluid with $Pr_1 = 10$.

In this analysis, most of the stability results predicted and selected from the Stability Map (Fig. 5(b)) are in accordance with the simulations obtained by the MODELICA model. It can be noticed that at power $Q = 1$ kW for fluid with $Pr_1 = 5$ (Table 5) and at power $Q = 7.5$ kW for fluid with $Pr_1 = 10$ (Table 6), results predicted by Stability Map are different from results obtained through DYMOLA® simulation. This region is characterized by the transition zone from laminar to turbulent regime for the secondary fluid, as its Reynolds number value is $Re_2 \approx 2530$, and it corresponds to the thin unstable line at $Re_1 \approx 1900$ that can be observed in the Stability Map (Fig. 5). Stability Map predicts that for this Reynolds value, $Re_1 \approx 1900$, instability occurs. The inaccuracy of the Stability Map to catch the right Reynolds value, predicted by the DYMOLA® simulation, can be associated with the fact of the linearization of the Natural Circulation equations, which is a non-linear phenomenon. Thus, approximations are introduced which can conduct the propagation of some errors. In fact, in this analysis,

Table 5
Verification of results predicted by the Stability Map (Fig. 5) with DYMOLA® simulation for the stability analysis with primary fluid with $Pr_1 = 5$.

$Pr_1 = 5$			
Power Q (kW)	Reynolds number Re_1 (−)	Stability Map prediction	DYMOLA® simulation
0.3	1100	Stable	Stable
0.8	1770	Stable	Stable
1	1970	Unstable	Stable
1.5	2320	Stable	Stable
1.7	2400	Unstable	Unstable
9	3770	Unstable	Unstable

Table 6
Verification of results predicted by the Stability Map (Fig. 5) with DYMOLA® simulation for the stability analysis with primary fluid with $Pr_1 = 10$.

$Pr_1 = 10$			
Power Q (kW)	Reynolds number Re_1 (−)	Stability Map prediction	DYMOLA® simulation
0.3	390	Stable	Stable
0.8	630	Stable	Stable
1.5	850	Stable	Stable
3	1180	Stable	Stable
7.5	1760	Stable	Unstable
8	1810	Stable	Stable
10	1970	Stable	Stable
15	2230	Stable	Stable

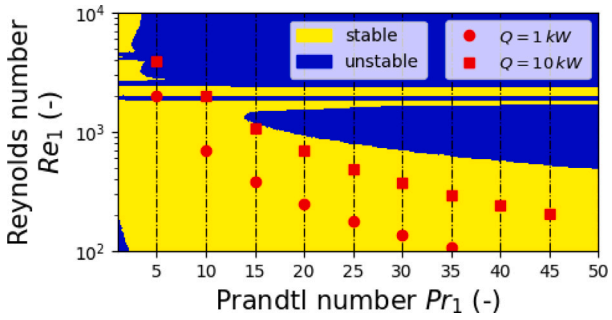

Fig. 15. Position of steady-state solution of CNCL in Stability Map (Fig. 5(b)) with temperature at the external cooler wall $T_c = 25\,°C$.

phenomena with order higher than the first one were not taken into account in Section 5. Moreover, in the MODELICA model of the heat exchanger (Fig. 7a), the external wall was not taken into account, unlike in the model developed for obtaining the Stability Map. Figs. 13 and 14 show the simulation results conducted with $Pr_1 = 5$ and $Pr_1 = 10$, respectively, where only the mass rates of the two loops are plotted. Regarding the unstable area in the Reynolds numbers of about 100 (Fig. 5(b)), the MODELICA model is not able to simulate the CNCL at very low power (less than 1 W) and the two fluids are practically static as very low velocities are reached, so it was not possible to verify that zone.

Concluding, the last study focused on the influence of heat power, cooler temperature and the fluid characteristics on the stability of the CNCL. Some steady-state points where obtained through the in-house Python code imposing the power at the heater $Q = 1\,kW$ and $Q = 10\,kW$ and the cooler temperature $T_c = 25\,°C$. The same thermophysical properties (ρ_f, c_f, k_f) where fixed as (54) for both primary and secondary fluids. To impose the Prandtl number of the desired primary fluid (Pr_1), the dynamic viscosity (μ_{f_1}) was varied to satisfy the Prandtl correlation (13), while the Prandtl number of the secondary fluid (Pr_2) was derived thanks to (47) by assuming $\overline{c} = 1$, $\overline{k} = 1$, $\overline{\mu}_f = 1$. Fig. 15 shows the position of the steady-state points, computed through the in-house code, in the Stability Map (Fig. 5(b)). At fixed thermophysical properties, an increase in the power of the heater has the effect of increasing the velocity of the fluid (Re_1 increases), approaching the system to the unstable zones. On the other hand, an increasing of the Prandtl number, at fixed heat power, has the effect of reducing the fluids regime (Re_1, Re_2 decrease). Finally, it has been noted that a temperature variation on the cooler's outer wall has a negligible effect on the Reynolds number, reflecting a very low variation of the same, which is hardly visible in the Stability Map.

8. Conclusions

In this work, the analytical studies carried out so far by [2,12] on the rectangular Single Natural Circulation Loops have been extended to the Coupled Natural Circulation Loops in order to study the stability of the system due to the influence of having both a distributed heat source as a heating system and an additional thermal inertia due to the presence of a coupled loop, a unique configuration of particular interest, the study of which requires the adoption of well-established analytical methods. As such, the DYNASTY-eDYNASTY facility is investigated in this paper by means of one-dimensional analysis and Perturbation Theory. This facility is unique in that it studies natural circulation conditions established in a Coupled Natural Circulation Loops (CNCLs) in presence of a distributed heat source as a promoter of circulation, which simulates the Internal Heat Generation condition that characterize, for example, in Molten Salt Fast Reactors.

The one-dimensional dynamic equations of conservation of laws for fluids, adopted by [2], has been extended to include the heat exchanger characteristics, adopted to couple the two Natural Circulation Loops. An in-house code has been developed in Python to determine the steady-states of the CNCLs under fixed operative conditions such as power delivered by the heater and cooler temperatures.

The study of the linear stability of these steady-states has been conducted by applying the Perturbation Theory to the dynamic equations. After linearization and non-dimensionalization of the equations obtained, the Stability Map was obtained as a function of the Reynolds and Prandtl numbers, which identify the steady-state of the fluid in the primary loop of the CNCLs. This map was compared against the one of Single Natural Circulation Loop counterpart. The Stability Map of the DYNASTY-eDYNASTY facility (CNCLs) shows an unstable behaviour when the heating power is increased, reaching turbulent regimes in the two loops, a phenomenon that is not found when looking at the stability map of the SNCL. In this unstable region, an oscillatory behaviour of the mass rates and temperature of both fluids was observed, which is

maintained by feedback phenomena. This fluctuation of state affects the efficiency: the mass rate of the loop increases due to the increase in the temperature of the fluid, which improves the heat transfer efficiency of the heat exchanger, thus the secondary loop (eDYNASTY loop) absorbs more heat. This increases the temperature of the secondary circuit and consequently the mass flow rate, further improving the heat transfer efficiency of the heat exchanger. The fluid in the primary loop is then cooled and its mass rate decreases, reducing the efficiency of heat transfer through the heat exchanger, and consequently increasing the temperature in the primary loop. This oscillatory behaviour of temperatures and mass rates is not dampened by the pressure drops of the loops, which try to stabilize the system, and the fluctuations are maintained. On the other hand, in the laminar regime, the unstable zone is reduced when comparing the Stability Maps of CNCLs and SNCLs, reflecting a stabilizing effect given by the coupling of a secondary Natural Circulation Loop.

The study then focused on the verification of the steady states and their stability predicted by the in-house code against simulations performed by a validated MODELICA model of the DYNASTY-eDYNASTY facility. Firstly, a series of steady states were calculated using the in-house code and the MODELICA model by fixing the thermo-physical properties of the fluids and the cooler temperature, and varying the heating power. The temperatures and mass rates calculated by the in-house code showed satisfactory agreement with those obtained by MODELICA for each steady state.

Then, some points were selected from the Stability Map and their state was verified with the MODELICA model predictions. From the verification, it was noticed that the Stability Map can predict the stable and unstable states of the system with satisfactory precision if compared with the DYMOLA® simulations results, confirming the reliability of the analytical procedure adopted to obtain the Stability Map. Some inconsistencies were found in the transition region from laminar to turbulent regimes of the fluids of both loops, due to the approximations introduced in the model developed to obtain the stability map.

Finally, plotting some steady-state points on the Stability Map, obtained from the in-house code by varying either the heating power of the primary loop or the Prandtl numbers of the fluids, confirmed that the system tended to move into unstable zones of the map as the heating power increased, reflecting an increase in the Reynolds number of the fluids. On the other hand, varying the Prandtl numbers while keeping the heating power constant resulted in a decrease of the Reynolds numbers.

Regarding future case studies, in anticipation of experimental campaigns of the DYNASTY-eDYNASTY facility for the validation process, the adiabaticity of the pipes is no longer acceptable and heat losses can be taken into account to be more coherent with the actual design of the facility, considering the planned insulation of the structure. Moreover, a fan cooler model must be implemented to have a more reliable model with respect to the facility. The Stability Map verification must be extended to more points of the map, for higher Reynolds and Prandtl numbers. In addition, in the stability analysis concentrated pressure losses and the cooler of the primary loop must be included, to get a model of the Coupled Natural Circulation Loops more realistic to the DYNASTY-eDYNASTY facility.

CRediT authorship contribution statement

Elia Novarese: Writing – review & editing, Writing – original draft, Visualization, Validation, Methodology, Formal analysis, Conceptualization. **Gabriele Benzoni:** Writing – review & editing, Validation, Supervision. **Carolina Introini:** Writing – review & editing, Validation, Supervision. **Stefano Lorenzi:** Writing – review & editing, Validation, Supervision. **Laura Savoldi:** Writing – review & editing, Visualization, Supervision. **Antonio Cammi:** Writing – review & editing, Visualization, Validation, Supervision, Conceptualization.

Declaration of competing interest

The authors declare that they have no known competing financial interests or personal relationships that could have appeared to influence the work reported in this paper.

Data availability

Data will be made available on request.

References

[1] IAEA, Use of Passive Safety Features in Nuclear Power Plant Designs and their Safety Assessment. URL: https://www.iaea.org/topics/design-safety-nuclear-power-plants/passive-safety-features.

[2] A. Cammi, L. Luzzi, A. Pini, The influence of the wall thermal inertia over a single-phase natural convection loop with internally heated fluids, Chem. Eng. Sci. 153 (2016) 411–433, http://dx.doi.org/10.1016/j.ces.2016.06.060, URL: https://www.sciencedirect.com/science/article/pii/S0009250916303554.

[3] A. Dass, S. Gedupudi, 1-D semi-analytical modeling and parametric study of a single phase rectangular coupled natural circulation loop, Chem. Eng. Sci. 207 (2019) 105–129, http://dx.doi.org/10.1016/j.ces.2019.05.050, URL: https://www.sciencedirect.com/science/article/pii/S0009250919304889.

[4] A. Pini, A. Cammi, L. Luzzi, Analytical and numerical investigation of the heat exchange effect on the dynamic behaviour of natural circulation with internally heated fluids, Chem. Eng. Sci. 145 (2016) 108–125, http://dx.doi.org/10.1016/j.ces.2016.01.014, URL: https://www.sciencedirect.com/science/article/pii/S0009250916000233.

[5] D. Ruiz, A. Cammi, L. Luzzi, Dynamic stability of natural circulation loops for single phase fluids with internal heat generation, Chem. Eng. Sci. 126 (2015) 573–583, http://dx.doi.org/10.1016/j.ces.2014.12.050, URL: https://www.sciencedirect.com/science/article/pii/S0009250914007696.

[6] G. Benzoni, C. Introini, S. Lorenzi, L. Loi, A. Cammi, 1D modelling and preliminary analysis of the coupled DYNASTY–eDYNASTY natural circulation loop, Front. Energy Res. 11 (2023) http://dx.doi.org/10.3389/fenrg.2023.1165179, URL: https://www.frontiersin.org/articles/10.3389/fenrg.2023.1165179.

[7] L. Luzzi, M. Misale, F. Devia, A. Pini, M. Cauzzi, F. Fanale, A. Cammi, Assessment of analytical and numerical models on experimental data for the study of single-phase natural circulation dynamics in a vertical loop, Chem. Eng. Sci. 162 (2017) 262–283, http://dx.doi.org/10.1016/j.ces.2016.12.058, URL: https://www.sciencedirect.com/science/article/pii/S0009250916307229.

[8] G. Benzoni, C. Introini, S. Lorenzi, A. Cammi, Preliminary validation of the 1D modeling of the DYNASTY natural circulation loop against results from water experimental campaign, Prog. Nucl. Energy 155 (2023) 104486, http://dx.doi.org/10.1016/j.pnucene.2022.104486, URL: https://www.sciencedirect.com/science/article/pii/S0149197022003602.

[9] J. Serp, M. Allibert, O. Beneš, S. Delpech, O. Feynberg, V. Ghetta, D. Heuer, D. Holcomb, V. Ignatiev, J.L. Kloosterman, L. Luzzi, E. Merle-Lucotte, J. Uhlíř, R. Yoshioka, D. Zhimin, The molten salt reactor (MSR) in generation IV: Overview and perspectives, Prog. Nucl. Energy 77 (2014) 308–319, http://dx.doi.org/10.1016/j.pnucene.2014.02.014, URL: https://www.sciencedirect.com/science/article/pii/S0149197014000456.

[10] Y.S. Jeong, S.B. Seo, I.C. Bang, Natural convection heat transfer characteristics of molten salt with internal heat generation, Int. J. Therm. Sci. 129 (2018) 181–192, http://dx.doi.org/10.1016/j.ijthermalsci.2018.01.036, URL: https://www.sciencedirect.com/science/article/pii/S1290072917316599.

[11] A. Pini, Analytical and Numerical Investigation of Single-Phase Natural Circulation Dynamics in Presence of Distributed Heat Sources (Ph.D. thesis), Politecnico di Milano, 2017, URL: https://www.politesi.polimi.it/handle/10589/133197.

[12] M.T. Cauzzi, Modelling and Experimental Investigation of Natural Circulation in Presence of Distributed Heating (Ph.D. thesis), Politecnico di Milano, 2019, URL: https://www.politesi.polimi.it/handle/10589/150619.

[13] D. Elton, U. Arunachala, P. Vijayan, Stability performance of series coupled natural circulation system with different operating procedures, Int. J. Therm. Sci. 179 (2022) 107693, http://dx.doi.org/10.1016/j.ijthermalsci.2022.107693, URL: https://www.sciencedirect.com/science/article/pii/S1290072922002289.

[14] T.L. Bergman, A.S. Lavine, F.P. Incropera, D.P. Dewitt, Fundamental of Heat and Mass Transfer, John Wiley & Sons, Inc., 2011.

[15] B. Stutz, P. Reghem, O. Martinez, Friction losses for flow of concentrated slurries, in: Second Workshop on Ice Slurries of IIF/IIR, No. 1, Paris, 2000.

[16] SciPy, Scipy.optimize.root_broyden2 Documentation. URL: https://docs.scipy.org/doc/scipy/reference/optimize.root-broyden2.html.

[17] N. Nise, Control Systems Engineering, sixth ed., John Wiley & Sons, Incorporated, 2011.

[18] J.J. Moré, D.C. Sorensen, Computing a trust region step, SIAM J. Sci. Stat. Comput. 4 (1983) 553–572, URL: https://api.semanticscholar.org/CorpusID:56112357.
[19] MATLAB, 2023. URL: https://www.mathworks.com.
[20] DYMOLA, 2023. Software. URL: https://www.3ds.com/products-services/catia/products/dymola/.
[21] P.A. Fritzson, Principles of object-oriented modeling and simulation with modelica 3.3: A cyber-physical approach, 2014, URL: https://api.semanticscholar.org/CorpusID:60060938.
[22] F. Casella, A. Leva, Modelling of thermo-hydraulic power generation processes using modelica, Math. Comput. Model. Dyn. Syst. 12 (1) (2006) 19–33, http://dx.doi.org/10.1080/13873950500071082.
[23] F.E. Cellier, E. Kofman, Continuous System Simulation, Springer Science & Business Media, 2006.
[24] IAPWS/IF-97, Release on the IAPWS industrial formulation 1997 for the thermodynamic properties of water and steam (IAPWS-IF97), 1997, URL: http://www.iapws.org/relguide/IF97-Rev.html.